ISTANBUL TECHNICAL UNIVERSITY ★ GRADUATE SCHOOL

SEISMIC RESPONSE ASSESSMENT OF A REINFORCED CONCRETE STRUCTURE USING DIFFERENT TYPES OF SEISMIC ISOLATORS

M.Sc. THESIS

Demet OKUROĞLU

Department of Civil Engineering

Structural Engineering Programme

JANUARY 2026

ISTANBUL TECHNICAL UNIVERSITY ★ GRADUATE SCHOOL

SEISMIC RESPONSE ASSESSMENT OF A REINFORCED CONCRETE STRUCTURE USING DIFFERENT TYPES OF SEISMIC ISOLATORS

M.Sc. THESIS

Demet OKUROĞLU
(501221037)

Department of Civil Engineering

Structural Engineering Programme

Thesis Advisor: Assoc. Prof. Dr. Arcan YANIK

JANUARY 2026

ISTANBUL TEKNİK ÜNİVERSİTESİ ★ LİSANSÜSTÜ EĞİTİM ENSTİTÜSÜ

FARKLI SİSMİK İZOLATÖR TİPLERİ KULLANILARAK BETONARME BİR YAPININ SİSMİK TEPKİSİNİN DEĞERLENDİRİLMESİ

YÜKSEK LİSANS TEZİ

Demet OKUROĞLU
(501221037)

İnşaat Mühendisliği Anabilim Dalı

Yapı Mühendisliği Programı

Tez Danışmanı: Doç. Dr. Arcan YANIK

OCAK 2026

Demet OKUROĞLU, a M.Sc. student of ITU Structural Engineering student ID 501221037, successfully defended the thesis/dissertation entitled "SEISMIC RESPONSE ASSESSMENT OF A REINFORCED CONCRETE STRUCTURE USING DIFFERENT SEISMIC ISOLATOR TYPES", which he/she prepared after fulfilling the requirements specified in the associated legislations, before the jury whose signatures are below.

Thesis Advisor :	**Assoc. Prof. Dr. Arcan YANIK** İstanbul Technical University	....
Jury Members :	**Prof. Dr. Fethi KADIOĞLU** İstanbul Technical University	....
	Assoc. Prof. Dr. Zafer KÜTÜĞ Yıldız Technical University	....

Date of Submission : 02 January 2026
Date of Defense : 19 January 2026

To my family,

FOREWORD

I would like to express my sincere and profound gratitude to my esteemed advisor, Assoc. Prof. Dr. Arcan Yanık, for his invaluable guidance, continuous support, and insightful contributions throughout every stage of this study. His academic expertise, constructive feedback, and encouragement have played a crucial role in the successful completion of this research.

I would also like to extend my deepest and heartfelt thanks to my family for their unwavering support, patience, and encouragement throughout this challenging journey. Their understanding, belief in me, and constant moral support provided the strength and motivation I needed to overcome the difficulties encountered during the research and writing process. Without their love and reassurance, the completion of this work would not have been possible.

January 2026

Demet OKUROĞLU
(Civil Engineer)

TABLE OF CONTENTS

Page

FOREWORD .... **ix**
TABLE OF CONTENTS .... **xi**
ABBREVIATIONS .... **xiii**
SYMBOLS .... **xv**
LIST OF TABLES .... **xvii**
LIST OF FIGURES .... **xix**
SUMMARY .... **xxi**
ÖZET .... **xxv**
1. INTRODUCTION **1**
1.1 Structural Control Systems 2
1.1.1 Active control systems 2
1.1.2 Semi-active control systems 3
1.1.3 Hybrid control systems 4
1.1.4 Passive control systems 5
1.1.5 Seismic isolation 6
1.1.5.1 Elastomeric (rubber-based) seismic isolation systems 9
1.2 Overview of Seismic Isolation 11
1.2.1 Literature review 11
1.2.2 Purpose of the thesis 15
2. DESIGN OF BUILDINGS WITH SEISMIC ISOLATION ACCORDING TO TSC-2018 .... **17**
2.1 Fundamental Principles of Design 17
2.2 Load Combinations 18
2.3 Design Principles of the Isolation System 18
2.3.1 Elastomeric isolation system 18
2.3.2 Lower and upper bound values to be used in design 19
2.3.3 Unit deformation limits of elastomeric isolation system 20
2.3.4 Vertical stability of elastomeric isolation system 21
2.3.5 Fundamental characteristics of elastomeric isolation system 23
3. NUMERICAL EXAMPLE **27**
3.1 Modelling 27
3.1.1 Material properties 28
3.1.2 Identification of structural system elements 28
3.1.3 Load combinations 31
3.1.4 Processing and preparation of strong ground motion records for structure analysis 32
3.1.5 Matching of earthquake records to the design spectrum 36
3.1.6 Identification of the seismic isolators 39
3.1.7 Lead rubber bearing (LRB) 40
3.1.8 High damping rubber bearing (HDRB) 41
4. ANALYSIS RESULTS UNDER SEISMIC LOADING **43**
4.1 Time-History Analysis of the Kocaeli Earthquake 44

4.2 Time-History Analysis of the Landers Earthquake 49
4.3 Time-History Analysis of the Kocaeli Earthquake with Reduced Material Strentgh.. 53
4.4 Time-History Analysis of the Landers Earthquake with Reduced Material Strength.. 59
5. CONCLUDING REMARKS AND RECOMMENDATIONS 65
REFERENCES 69
APPENDICES 79
CURRICULUM VITAE 81

ABBREVIATIONS

LRB	: Lead Rubber Bearing
HDRB	: High Damping Rubber Bearing
TSC	: Turkish Seismic Code
MR	: Magneto-Rheological
SBI	: Smart Seismic Isolation
ENR	: Engineering News Record
U-FREI	: Unconnected Fiber Reinforced Elatomeric Isolators
TMD	: Tuned Mass Damper
SMARB	: Shape Memory Alloy Rubber Bearing
CFST	: Circular Hollow Section
CES	: Concrete Encased Steel
RC	: Reinforced Concrete
PREIs	: Perforated-Reinforced Elastometric Isolators
TFI	: Tuned Fluid Inerter
VFPB	: Variable Friction Pendulum Bearing
FPS	: Friction Pendulum System
SMA	: Shape Memory Alloy
SMRs	: Small Modular Reactor
DS-HVDB	: Double-Sided Sliding Horizontal-Vertical Decoupling Seismic Isolation Bearing
FPB	: Friction Pendulum Bearing
BI	: Base Isolation
TFI	: Tuned Fluid Inerter
FS	: Friction Slider
DD-1	: Design Earthquake Ground Motion Level-1
DD-2	: Design Earthquake Ground Motion Level-2
DD-3	: Design Earthquake Ground Motion Level-3
DD-4	: Design Earthquake Ground Motion Level-4
KCE	: Lead Rubber Bearing
YSE	: High Damping Rubber Bearing

TS 500	**:** Requirements for Design and Construction of Reinforced Concrete Structures
TS 708	**:** Steel for the Reinforcement of Concrete
IO	**:** Immediate Occupancy
LD	**:** Limited Damage
DGT	**:** Strength-Based Design
RSN 1166	**:** Earthquake Record Sequence Number (Kocaeli)
RSN 864	**:** Earthquake Record Sequence Number (Landers)
AFAD	**:** Disaster and Emergency Management Authority
PEER	**:** Pacific Earthquake Engineering Research Center
B420C	: High-Ductility Ribbed Reinforcing Steel
C30	: Concrete with Characteristic Compressive Strength of 30 Mpa
BC1	: Plain (Smooth) Reinforcing Steel
C15	: Concrete with Characteristic Compressive Strength of 15 Mpa

SYMBOLS

Q	**:** Live Load
G	**:** Dead Load
S	**:** Snow Load
H	**:** Horizontal Ground Pressure
$\mathbf{E_d^{(H)}}$	**:** Horizontal Seismic Effect
$\mathbf{E_d^{(Z)}}$	**:** Vertical Seismic Effect
$\mathbf{F_Q}$	**:** Lead-Rubber Bearing's Characteristic Strength
$\mathbf{k_2}$	**:** Lead-Rubber Bearing's Post-Elastic Stiffness
λ_{upper}	**:** Yield the Upper and Lower Bound Values of the Isolation System Parameters
λ_{lower}	**:** Yield the Upper and Lower Bound Values of the Isolation System Parameters
λ_{ae}, λ_{test}, λ_{spec}	**:** Aging And Environmental Impacts, Testing Conditions, and Manufacturing Variability Parameters of the Isolation System
$\mathbf{P_{K1}}$	**:** Vertical Force Obtained Under the Load Combination
$\mathbf{A_r}$	**:** Area of a Single Elastomer Layer Bonded to Steel Plates
$\mathbf{E_c}$	: Compressive Modulus
$\mathbf{\Delta_s}$	: Horizontal Displacement Resulting From Horizontal Loading
$\mathbf{T_r}$	: The Total Thickness of the Elastomer Layers
θ_s	: The Design Rotation Angle
B	: Diameter of the Elastomer Bonded to the Steel Plate
t	: Represents the Thickness of an Individual Elastomer Layer
$\mathbf{P_{K2}}$	: Vertical Force Obtained Under the Load Combination
ε_b	: Vertical Force Obtained Under the Load Combination
$\mathbf{P_{cr}}$	: The Buckling Load of Elastomeric Isolation
$\mathbf{G_v}$	: The Shear Modulus Of The Elastomer Material
$\mathbf{B_L}$	: The Diameter of the Lead Core
D	: Displacement
$\mathbf{k_1}$	: Initial Elastic Stiffness

k_2 : Secondary Stiffness

F_y : Effective Yield Strength

D_y : Effective Yield Displacement

β_e : The Effective Damping Ratio

W_d : The Energy Dissipated During A Loading Cycle

A_L : Lateral Surface Area of the Elastomer Layer

B_L : The Diameter of the Lead Core

k_v : Vertical Stiffness

E_V : The Vertical Stiffness Modulus

K : The Rubber Material's Bulk Modulus

E_0 : The Rubber Material's Elastic Modulus

LIST OF TABLES

Page

Table 2.1 : Earthquake ground motion levels (TSC,2018). **17**
Table 2.2 : Recommended lower and upper bound values of strength and stiffness parameters for elastomeric isolation system (TSC, 2018)...................... **19**
Table 3.1 : Effective section stiffness modification factors (TSC, 2018). **29**
Table 3.2 : Performance targets and applicable evaluation/design approaches for seismically isolated buildings according to seismic design categories (TSC, 2018). **30**
Table 3.3 : Earthquake load reduction and overstrength factors (TSC, 2018).......... **31**
Table 3.4 : Earthquake load reduction and overstrength factors (TSC, 2018).......... **31**
Table 3.5 : Design spectrum parameters selected for the Bahçelievler/İstanbul region. **37**
Table 3.6 : LRB design parameters. **41**
Table 3.7 : HDRB design parameters. **42**
Table 4.1 : Comparison of structural period, base shear, and overturning moment of the models under the Kocaeli Earthquake. **44**
Table 4.2 : Comparison of structural period, base shear, and overturning moment of the models under the Landers Earthquake.. **49**
Table 4.3 : Comparison of structural period, base shear, and overturning moment models under the Kocaeli Earthquake with reduced material strength. . **54**
Table 4.4 : Comparison of structural period, base shear, and overturning moment under the Kocaeli Earthquake with reduced material strength models. . **59**

LIST OF FIGURES

Page

Figure 1.2 : The general working principle of passive control systems. (Constantinou et al., 1998). **5**
Figure 1.3 : The horizontal elastic design acceleration spectrum (TSC, 2018). **7**
Figure 1.4 : Impact of period elongation obtained by seismic isolation on accelerations (Constantinou et al., 2007). **8**
Figure 1.5 : Impact of period elongation obtained by seismic isolation on displacements (Constantinou et al., 2007). **8**
Figure 1.6 : Low damping rubber bearing (URL-3). **9**
Figure 1.7 : High damping rubber bearing (URL-4). **10**
Figure 1.8 : Lead rubber bearing (URL-5). **11**
Figure 2.1 : Parameters used in the calculation A_{re} (TSC,2018). **22**
Figure 2.2 : Elastomeric isolator units composed of alternating layers of steel and natural rubber (or neoprene) plates (TSC, 2018). **23**
Figure 2.3 : Simplified force–displacement (loading cycle) curve of the isolation system (TSC, 2018). **24**
Figure 3.1 : Structural model of the building. **30**
Figure 3.2 : Acceleration–time plot of earthquake record RSN 1166 (Kocaeli). **33**
Figure 3.3 : Velocity–time plot of earthquake record RSN 1166 (Kocaeli). **34**
Figure 3.6 : Velocity–time plot of earthquake record RSN 864 (Landers). **35**
Figure 3.7 : Displacement–time plot of earthquake record RSN 864 (Landers). **36**
Figure 3.8 : Comparison of the Kocaeli Earthquake spectrum with the design spectrum. **38**
Figure 3.10 : Comparison of the Landers Earthquake spectrum with the design spectrum. **39**
Figure 3.11 : Comparison of the Landers Earthquake acceleration with the design accelerations. **39**
Figure 3.12 : LRB layers (URL-2). **40**
Figure 3.13 : HDRB layers (URL-2). **42**
Figure 4.1 : Structural model with LRB. **43**
Figure 4.2 : Structural model with HDRB. **44**
Figure 4.3 : Distribution of maximum story displacements under the Kocaeli Earthquake. **46**
Figure 4.4 : Top-story displacement–time plots under the Kocaeli Earthquake. **47**
Figure 4.5 : Distribution of maximum velocities under the Kocaeli Earthquake. **47**
Figure 4.6 : Top-story velocity–time plots under the Kocaeli Earthquake. **48**
Figure 4.7 : Distribution of maximum story accelerations under the Kocaeli Earthquake. **48**
Figure 4.8 : Top-story acceleration–time plots of under the Kocaeli Earthquake. **49**

Figure 4.9 : Distribution of maximum story relative displacement under the Landers Earthquake. **51**
Figure 4.10 : Top-story displacement–time plots under the Landers Earthquake. .. **51**
Figure 4.11 : Distribution of maximum velocities under the Landers Earthquake. . **52**
Figure 4.12 : Top-story velocity–time plots under the Landers Earthquake. **52**
Figure 4.13 : Distribution of maximum story accelerations under the Landers Earthquake. **53**
Figure 4.14 : Top-story acceleration–time plots under the Landers Earthquake. **53**
Figure 4.15 : Distribution of maximum story displacements under the Kocaeli Earthquake with reduced material strength. **56**
Figure 4.16 : Top-story displacement–time plots under the Kocaeli Earthquake with reduced material strength. **56**
Figure 4.17 : Distribution of maximum velocities under the Kocaeli Earthquake with reduced material strength. **57**
Figure 4.18 : Top-story velocity–time plots under the Kocaeli Earthquake with reduced material strength **57**
Figure 4.19 : Distribution of maximum story accelerations under the Kocaeli Earthquake with reduced material strength. **58**
Figure 4.20 : Top-story acceleration–time plots under the Kocaeli Earthquake with reduced material strength. **59**
Figure 4.21 : Distribution of maximum story displacements under the Landers Earthquake with reduced material strength. **61**
Figure 4.22 : Top-story displacement–time plots under the Landers Earthquake with reduced material strength. **61**
Figure 4.23 : Distribution of maximum velocities under the Landers Earthquake with reduced material strength. **62**
Figure 4.24 : Top-story velocity–time plots under the Landers Earthquake with reduced material strength. **63**
Figure 4.25 : Distribution of maximum story accelerations under the Landers Earthquake with reduced material strength. **64**
Figure 4.26 : Top-story acceleration–time plots under the Landers Earthquake with reduced material strength. **64**

SEISMIC RESPONSE ASSESSMENT OF A REINFORCED CONCRETE STRUCTURE USING DIFFERENT TYPES OF SEISMIC ISOLATORS

SUMMARY

Throughout human history, earthquakes have been among the most destructive natural disasters. The dynamic behavior of structures is directly impacted by the energy produced as a result of abrupt cracks in the Earth's crust, which travel to the surface as seismic waves.Turkey’s location on active fault lines makes earthquake hazard a constant and unavoidable reality. The inability to precisely predict the time, magnitude, and impact of earthquakes necessitates that structures be designed not only with the objective of preventing collapse, but also in accordance with performance targets that prioritize life safety, reduction of economic losses, and post-earthquake functionality. Major earthquakes occurring particularly in densely populated areas have revealed the limitations of conventional design approaches and clearly demonstrated the need for more effective engineering solutions.

In order to diffuse earthquake energy within the structural system, the traditional seismic design technique is predicated on making structural parts stronger and more ductile. In this method, seismic energy is directly transmitted to the superstructure, and certain levels of damage are accepted. Although ensuring life safety is the primary objective, preserving the functionality of the structure after an earthquake cannot be guaranteed. Particularly for buildings that need to continue functioning following an earthquake, such as hospitals, emergency response centers, fire stations, data centers, and key infrastructure sites, this strategy is inadequate.For this reason, structural control methods, particularly seismic isolation systems classified as passive control systems, have come to the forefront.

By separating the structure from its foundation, seismic isolation systems work on the basic tenet of minimizing the transfer of seismic energy to the superstructure. The isolators used in these systems are designed to provide high vertical stiffness and low horizontal stiffness. This lengthens the structure's natural vibration period and moves the system away from the ground motion's dominating frequency range. Story accelerations, velocities, and internal force demands all drastically diminish as a result of the period elongation, which also lessens base shear forces and bending moments pressing on the structure. However, greater displacements at the isolation level could result from the period's extension. Therefore, the damping capacity of the isolators is of critical importance. Because of its great damping capacity, the structure's post-earthquake functionality is maintained while maximum and residual displacements are kept under control.

In the first stage of this study, previous research was reviewed and seismic isolation systems were introduced. The literature indicates that elastomer-based isolators are widely preferred due to their high energy dissipation capacity and ease of application. The performance evaluation of two distinct elastomer-based seismic isolation systems lead rubber bearing (LRB) and high damping rubber bearing (HDRB) systems is the primary emphasis of in this context. While the lead core's yielding behavior in the LRB

system results in a hysteretic mechanism for energy dissipation, specifically compounded rubber with a high inherent damping capacity provides continuous and consistent energy dissipation in the HDRB system.

A model of a seven-story reinforced concrete building was created as part of the study. SAP2000 software was used to quantitatively assess how base isolation affected structural behavior. The analysis method used was nonlinear time history analysis. This method enables the direct application of time-dependent acceleration records of real earthquakes to the model and allows realistic investigation of the inelastic behavior of the structure.

The 1999 Kocaeli and 1992 Landers earthquake records obtained from the PEER database were used as ground motion inputs. The selected records were scaled in accordance with the target design spectra defined by AFAD, and spectrum matching was performed using the SeismoMatch program. As a result, it was guaranteed that the ground motions utilized in the analysis accurately reflected the level of seismic threat. The performance of fixed-base structures was compared to that of LRB- and HDRB-isolated structures under a variety of earthquake records.

Additionally, models with varying levels of material strength were developed for the same structural geometry in order to examine how differences in structural material strength affect the efficacy of seismic isolation systems. In the first model, C30 concrete and B420C reinforcing steel representing new design conditions were used. The low strength levels commonly found in the existing building stock were represented in the second model by using C15 concrete and BC1 reinforcing steel. Thus, the effectiveness of seismic isolation systems was evaluated not only for newly designed structures but also for existing structures with limited material capacity.

Base shear force, base bending moment, maximum displacement, story accelerations, story velocities, and natural vibration periods were taken into consideration as the main criteria in the performance evaluation. The first natural vibration period of the fixed-base construction was found to be 0.60 seconds based on the analytical results. When the LRB system was used, this period increased to 1.77 s, corresponding to an increase of approximately 195%. In the HDRB system, the fundamental period reached 2.38 s, representing an increase of approximately 297%. This notable period elongation suggests that the structure's effective horizontal stiffness has decreased and that the superstructure receives earthquake energy at lower frequencies.

Both isolation methods offered notable decreases in base shear force and base moment values when compared to the fixed-base model. Because of its strong inherent damping capability, the HDRB system was specifically found to be more successful than the LRB system in lowering force demands. In the analyses conducted under the Kocaeli and Landers earthquake records, the fixed-base model produced the highest base shear force and moment values, whereas these values were significantly reduced in the LRB and HDRB models. Because of the energy dissipation mechanism based on the lead core yielding, the LRB system demonstrated noticeable hysteretic behavior and helped to manage the consumption of earthquake energy. The performance of the structure was positively impacted by this attribute, especially when there were prolonged ground motions. The HDRB system, on the other hand, demonstrated a more balanced and continuous energy dissipation behavior, reducing internal force demands in the superstructure more effectively. However, in some analysis cases, it produced lower residual displacement values compared to the LRB system.

Analysis of story velocities and accelerations revealed that acceleration values were focused in the upper stories and rose with the fixed-base model's height. In the isolated models, accelerations were significantly reduced and seismic demands were concentrated at the isolation level. This provides a significant advantage in terms of reducing the risk of damage in superstructure elements.

In the C15–BC1 model with reduced material strength, significant increases were observed in force and deformation demands in the fixed-base system. In contrast, in the LRB- and HDRB-isolated models, the reduction in material strength had a limited effect on structural response. It was observed that in isolated systems, behavior was largely controlled by the properties of the isolators, and the decrease in superstructure material capacity did not dramatically affect overall performance. According to this research, seismic isolation techniques show a great deal of promise for fortifying the existing stock of buildings.

Overall, the seismic performance of the structure was shown to be greatly enhanced by both isolation technologies. While the LRB system demonstrated controlled and steady behavior due to its hysteretic energy dissipation capabilities, the HDRB system produced more effective outcomes in terms of force reduction and acceleration control. The system should be selected according to project-specific performance objectives, including force reduction targets, energy dissipation mechanism, displacement capacity, maintenance requirements, and expected performance criteria.

This study demonstrates that seismic isolation systems provide an effective solution for both newly designed structures and existing building stock with low material strength. In future studies, consideration of different earthquake records, soil–structure interaction, temperature variations, aging effects, and economic analyses, as well as comparison of different isolation types, will contribute to a more comprehensive evaluation of seismic isolation systems.

FARKLI SİSMİK İZOLATÖR TİPLERİ KULLANILARAK BETONARME BİR YAPININ SİSMİK TEPKİSİNİN DEĞERLENDİRİLMESİ

ÖZET

İnsanlık tarihi boyunca depremler en yıkıcı doğal afetler arasında yer almıştır. Yer kabuğundaki ani kırılmalar sonucu açığa çıkan enerji, yüzeye sismik dalgalar halinde yayılmakta ve yapıların dinamik davranışını doğrudan etkilemektedir. Türkiye'nin sismik açıdan aktif tektonik kuşaklar üzerinde konumlanması, deprem riskini ülke için süreklilik gösteren ve göz ardı edilemez bir olgu haline getirmektedir. Depremlerin zamanının, büyüklüğünün ve etkisinin kesin olarak tahmin edilememesi, yapıların yalnızca göçmenin önlenmesi yaklaşımıyla değil; aynı zamanda can güvenliğini, ekonomik kayıpların azaltılmasını ve kullanım sürekliliğini esas alan performans hedefleri doğrultusunda tasarlanmasını zorunlu kılmaktadır. Özellikle yoğun yerleşim alanlarında meydana gelen büyük depremler, geleneksel tasarım anlayışının sınırlarını ortaya koymuş ve daha etkin mühendislik çözümlerine olan ihtiyacı açıkça göstermiştir.

Geleneksel deprem tasarım yaklaşımı, yapı elemanlarının dayanımını ve sünekliğini artırarak deprem enerjisinin yapı bünyesinde karşılanmasını esas almaktadır. Bu yöntemde deprem enerjisi doğrudan üstyapıya iletilmekte ve belirli hasar seviyeleri kabul edilmektedir. Can güvenliğinin sağlanması temel hedef olmakla birlikte, deprem sonrasında yapının kullanılabilirliğinin korunması garanti edilememektedir. Özellikle hastaneler, acil müdahale merkezleri, itfaiye binaları, veri merkezleri ve kritik altyapılar gibi deprem sonrasında da işlevini sürdürmesi gereken yapılarda bu yaklaşım yetersiz kalmaktadır. Bu nedenle yapısal kontrol yöntemleri ve özellikle pasif kontrol sistemleri arasında yer alan sismik izolasyon sistemleri ön plana çıkmıştır.

Sismik izolasyon sistemlerinin temel prensibi, yapıyı temelden ayırarak deprem enerjisinin üstyapıya iletimini azaltmaktır. Bu sistemlerde kullanılan izolatörler, yüksek düşey rijitlik ve düşük yatay rijitlik sağlayacak şekilde tasarlanmaktadır. Böylece yapının doğal titreşim periyodu uzatılmakta ve sistem, yer hareketinin baskın frekans aralığından uzaklaştırılmaktadır. Periyot uzaması sayesinde yapıya etkiyen taban kesme kuvvetleri ve eğilme momentleri azalmakta; kat ivmeleri, hızları ve iç kuvvet talepleri önemli ölçüde düşmektedir. Bununla birlikte, periyodun uzaması izolasyon seviyesinde daha büyük yer değiştirmelere neden olabilmektedir. Bu nedenle izolatörlerin sönüm kapasitesi kritik önem taşımaktadır. Yüksek sönümleme kapasitesi sayesinde hem maksimum hem de artık yer değiştirmeler kontrol altına alınmakta ve yapının deprem sonrası kullanılabilirliği korunmaktadır.

Bu çalışmanın ilk aşamasında, önceki araştırmalar incelenmiş ve sismik izolasyon sistemleri tanıtılmıştır. Literatürde özellikle elastomer esaslı izolatörlerin, yüksek enerji sönümleme kapasitesi ve uygulama kolaylığı nedeniyle yaygın olarak tercih edildiği görülmektedir. Bu kapsamda tez çalışmasının temel odak noktası, elastomer esaslı iki farklı sismik izolasyon sistemi olan kurşun çekirdekli kauçuk izolatör (LRB) ve yüksek sönümlü kauçuk izolatör (HDRB) sistemlerinin performans değerlendirmesidir. LRB sisteminde enerji sönümleme, kurşun çekirdeğin akma davranışı sayesinde histeretik mekanizma ile sağlanırken; HDRB sisteminde yüksek doğal sönüm kapasitesine sahip özel kauçuk bileşimi sayesinde sürekli ve dengeli bir enerji tüketimi gerçekleşmektedir.

Çalışma kapsamında 7 katlı betonarme bir yapı modeli oluşturulmuştur. Taban izolasyonunun yapısal davranış üzerindeki etkileri SAP2000 yazılımı kullanılarak sayısal olarak değerlendirilmiştir. Bu çalışma kapsamında yapısal davranışın belirlenmesi amacıyla doğrusal olmayan zaman tanım alanı analizi uygulanmıştır. Bu yöntem, gerçek deprem kayıtlarının zamana bağlı ivme değerlerinin doğrudan modele uygulanmasını sağlamakta ve yapının elastik ötesi davranışının gerçekçi biçimde incelenmesine olanak tanımaktadır.

Deprem kayıtları olarak PEER veri tabanından temin edilen 1999 Kocaeli ve 1992 Landers depremleri kullanılmıştır. Seçilen kayıtlar, AFAD tarafından tanımlanan hedef tasarım spektrumlarına uygun şekilde ölçeklendirilmiş ve SeismoMatch programı kullanılarak spektrum uyumlaması gerçekleştirilmiştir. Böylece analizlerde kullanılan yer hareketlerinin ilgili deprem tehlike düzeyini temsil etmesi sağlanmıştır. Çeşitli deprem kayıtları altında sabit tabanlı yapıların performansı, LRB ve HDRB izolasyonlu yapıların performansı ile karşılaştırılmıştır.

Ayrıca yapısal malzeme dayanımındaki değişimlerin sismik izolasyon sistemlerinin etkinliği üzerindeki etkilerini incelemek amacıyla aynı yapı geometrisi için farklı malzeme dayanım seviyelerine sahip modeller oluşturulmuştur. İlk modelde yeni tasarım koşullarını temsil eden C30 beton ve B420C donatı çeliği kullanılmıştır. İkinci modelde ise mevcut yapı stoğunda sıklıkla karşılaşılan düşük dayanım seviyelerini temsil etmek amacıyla C15 beton ve BC1 donatı çeliği esas alınmıştır. Böylece sismik izolasyon sistemlerinin yalnızca yeni tasarlanan yapılar için değil, aynı zamanda mevcut ve malzeme kapasitesi sınırlı yapılar için de etkinliği değerlendirilmiştir.

Performans değerlendirmesinde taban kesme kuvveti, taban eğilme momenti, maksimum yer değiştirme, kat ivmeleri, kat hızları ve doğal titreşim periyotları temel parametreler olarak dikkate alınmıştır. Analiz sonuçlarına göre sabit tabanlı yapının birinci doğal titreşim periyodu 0.60 s olarak belirlenmiştir. LRB sistemi kullanıldığında bu periyot 1.77 s’ye yükselmiş ve yaklaşık %195 oranında artış göstermiştir. HDRB sisteminde ise temel periyot 2.38 s’ye ulaşmış ve yaklaşık %297 oranında artmıştır. Bu önemli periyot uzaması, yapının etkin yatay rijitliğinin azaldığını ve deprem enerjisinin üstyapıya daha düşük frekans aralığında iletildiğini göstermektedir.

Taban kesme kuvveti ve taban momenti değerleri açısından her iki izolasyon sistemi de sabit tabanlı modele kıyasla belirgin azalmalar sağlamıştır. Özellikle HDRB sistemi, yüksek doğal sönüm kapasitesi sayesinde kuvvet taleplerinin azaltılmasında LRB sistemine kıyasla daha etkili bulunmuştur. Kocaeli ve Landers deprem kayıtları altında yapılan analizlerde sabit tabanlı model en yüksek taban kesme kuvveti ve moment değerlerini üretirken, LRB ve HDRB modellerinde bu değerlerin önemli ölçüde azaldığı gözlemlenmiştir. LRB sistemi, kurşun çekirdeğin akma davranışına dayanan enerji sönümleme mekanizması sayesinde belirgin bir histeretik davranış sergilemiş ve deprem enerjisinin kontrollü biçimde tüketilmesine katkı sağlamıştır. Bu özellik özellikle uzun periyotlu yer hareketleri altında yapının performansını olumlu yönde etkilemiştir. HDRB sistemi ise daha dengeli ve sürekli bir enerji sönümleme davranışı göstererek üstyapıdaki iç kuvvet taleplerini daha etkin biçimde azaltmıştır. Ancak bazı analiz durumlarında LRB sistemine kıyasla daha düşük artık yer değiştirme değerleri üretmiştir.

Kat ivmeleri ve hızları incelendiğinde sabit tabanlı modelde ivme değerlerinin yapı yüksekliği boyunca arttığı ve üst katlarda yoğunlaştığı görülmüştür. İzolatörlü modellerde ise ivmelerin belirgin biçimde azaldığı ve sismik taleplerin izolasyon seviyesinde yoğunlaştığı belirlenmiştir. Bu durum, üstyapı elemanlarında hasar oluşma riskinin azaltılması açısından önemli bir avantaj sağlamaktadır.

Malzeme dayanımının düşürüldüğü C15–BC1 modelde sabit tabanlı sistemin kuvvet ve deformasyon taleplerinde belirgin artışlar meydana gelmiştir. Buna karşılık, LRB ve HDRB izolasyonlu modellerde malzeme dayanımındaki azalma yapısal tepki üzerinde sınırlı etki göstermiştir. İzolasyonlu sistemlerde davranışın büyük ölçüde izolatör özellikleri tarafından kontrol edildiği ve üstyapı malzeme kapasitesindeki düşüşün genel performansı dramatik biçimde etkilemediği görülmüştür. Bu bulgu, sismik izolasyon sistemlerinin mevcut yapı stokunun güçlendirilmesinde önemli bir potansiyele sahip olduğunu göstermektedir.

Genel değerlendirme sonucunda, her iki izolasyon sisteminin de yapının deprem performansını önemli ölçüde iyileştirdiği belirlenmiştir. HDRB sistemi kuvvet azaltımı ve ivme kontrolü açısından daha etkin sonuçlar verirken; LRB sistemi histeretik enerji tüketim kapasitesi ile kontrollü ve kararlı bir davranış sergilemiştir. Sistem seçiminin; kuvvet azaltımı hedefleri, enerji sönümleme mekanizması, yer değiştirme kapasitesi, bakım gereksinimleri ve proje özelindeki performans beklentileri doğrultusunda yapılması gerektiği sonucuna varılmıştır.

Bu çalışma, sismik izolasyon sistemlerinin hem yeni tasarlanacak yapılar hem de malzeme dayanımı düşük mevcut yapı stoğu için etkili bir çözüm sunduğunu ortaya koymaktadır. Gelecek çalışmalarda farklı deprem kayıtları, zemin-yapı etkileşimi, sıcaklık değişimleri, yaşlanma etkileri ve ekonomik analizlerin dikkate alınması; ayrıca farklı izolasyon türlerinin karşılaştırılması, sismik izolasyon sistemlerinin daha kapsamlı değerlendirilmesine katkı sağlayacaktır.

1. INTRODUCTION

Structures are subjected to a variety of external loads, including earthquakes, wind, and impact loads. Among these, earthquakes constitute a natural hazard that cannot be controlled and may result in significant destruction. Each major seismic event emphasizes the critical necessity for structures to possess sufficient resilience against seismic effects. In light of these unpredictable and uncertain hazards, buildings should be designed not only to prevent structural collapse but also to prioritize the protection of human life. Globally, approximately 500.000 earthquakes occur annually, of which around 100.000 are perceptible and approximately 100 cause structural damage (URL-1). This highlights the high likelihood of encountering ground motions with unpredictable magnitude and timing, underscoring the importance of standardized structural design regulations. In Turkey, the Turkish Building Earthquake Code provides the regulatory framework for structural analysis and design (TSC, 2018).

The Northridge Earthquake in 1994, the Kocaeli and Düzce earthquakes in 1999, the Christchurch and Tohoku-Oki Earthquakes in 2011, the Kumamoto Earthquake in 2016, the Puebla Earthquake in Mexico in 2017, the Sulawesi Earthquake in Indonesia in 2018, the Aegean Sea Earthquake in 2020 that affected Greece and Turkey, and the Kahramanmaraş Earthquake in 2023 each resulted in significant casualties (Al-Janabi et al., 2025). The urgent need for more resilient earthquake-resistant design solutions has been highlighted by these tragic disasters, which have shown serious vulnerabilities in buildings and infrastructure across numerous seismic regions. One of the most effective methods for designing earthquake-resistant structures is seismic isolation, which aims to lessen the seismic energy transmitted to the superstructure. By using isolators between the foundation and the superstructure, this technique creates an interface that reduces vibrations caused by earthquakes at the base and guarantees that the superstructure is subjected to as little seismic force as possible. This approach focuses on reducing the structural response to seismic excitations rather than increasing the inherent seismic capacity of the building. In key institutions where post-earthquake operational continuity is crucial, like hospitals, emergency response centers, and vital infrastructure, the use of seismic isolation has grown in significance. Furthermore, the use of seismic isolation is crucial for protecting human life and minimizing financial damages in heavily populated and quickly urbanizing areas.

1.1 Structural Control Systems

Conventional structures are designed with adequate damping, stiffness, and durability to withstand earthquake effects. Accordingly, traditional seismic design methods rely on predictive analysis models to minimize structural damage (Cercevik & Cercevik, 2025). However, the unpredictable timing and magnitude of earthquakes make it challenging to accurately estimate potential damage. Severe seismic events can threaten human life and property, leading to structural collapse and secondary disasters such as landslides and tsunamis (Zhong et al., 2024). For instance, on February 6, 2023, two major earthquakes with magnitudes of 7.7 and 7.6 struck Kahramanmaraş province in Türkiye, where both the intensity of the quakes and the insufficient preparedness of the building stock resulted in significant human and economic losses (Kandemir & Mortazavi, 2024). Similarly, China experienced the Wenchuan earthquake with a magnitude of 7.9 on May 12, 2008, along the eastern margin of the Tibetan Plateau, and Haiti suffered a magnitude 7.0 earthquake on January 12, 2010, its strongest on record, causing widespread structural collapse and numerous fatalities (Salaas et al., 2023). Implementing structural control systems is one practical way to improve the safety of both structural and non-structural elements and preserve the operational functionality of buildings after seismic occurrences. Furthermore, these systems include passive, active, semi-active, and hybrid control methods, while passive control devices have gained widespread use in the construction industry, primarily because they require no external power source and offer low installation and maintenance costs (Castillo et al., 2024).

1.1.1 Active control systems

Active control systems generally operate through hydraulic or electromechanical actuators, and their functioning is governed by appropriate control algorithms. These systems apply control forces to counteract external loads, thereby reducing the structural response through feedback mechanisms. The general working principle of active control systems is illustrated in Figure 1.1. According to Chang et al. (2018), to enhance performance and achieve more effective mitigation of base displacements, seismic isolation system can be integrated with active control devices (e.g., hydraulic actuators) using active control algorithms, thus providing efficient control and adaptability across a wide range of seismic excitations. The integration of seismic isolation with active control, commonly referred to as active seismic isolation, enables the simultaneous optimization of structural response, offering an effective reduction in both floor accelerations and base displacements (Chang & Spencer, 2010). Because active control systems rely on an external power source to generate control forces, their implementation is often constrained by the need for large-scale equipment, continuous feedback monitoring, and high energy consumption. Nevertheless, among the various structural control strategies, active seismic isolation system have emerged as one of the most promising approaches (Scruggs et al., 2006).

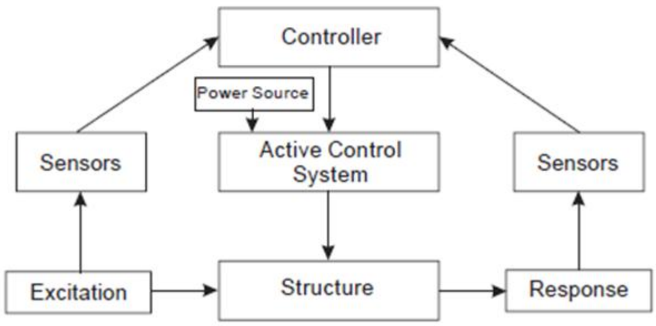

Figure 1.1 : The general working principle of active control system. (Constantinou et al., 1998).

1.1.2 Semi-active control systems

In order to safeguard structures against external excitations like wind and earthquakes, semi-active control systems include the key elements of both active and passive systems. Although they resemble active control methods, their primary distinction lies in the significantly lower demand for external energy compared to fully active systems. According to Mohebbi and Dadkhah (2019), semi-active control systems are preferred due to their adaptability and low power requirements. In addition, various types including magneto-rheological dampers, variable friction systems, variable orifice dampers, and piezoelectric friction dampers have been studied in conjunction with seismic isolation system, enhancing both system flexibility and effectiveness. Additionally, Mohebbi and Dadkhah (2017) found that combining semi-active and active control systems can result in an adaptive hybrid system that can successfully respond to various seismic events and reduce base drift. The primary distinction between active and semi-active control systems lies in their power requirements: while an active control system depends on a substantial external power source, a semi-active system requires only a limited power supply and is often battery-operated (Gutierrez Soto & Adeli, 2018). In particular, semi-active magneto-rheological (MR) dampers have attracted considerable attention, and both theoretical and experimental studies have demonstrated that they outperform conventional viscous dampers in terms of control effectiveness (Gao et al., 2021). Nevertheless, semi-active control requires both a sensor network and an external power source, which increases system complexity and limits its widespread implementation (Kim et al., 2010).

1.1.3 Hybrid control systems

These systems combine the benefits of active and passive techniques to improve overall structural safety. Hybrid systems are designed to overcome the limitations of passive control and to prevent excessive structural response under sudden loads. Seismic isolation has been shown to significantly reduce the structural reaction; nevertheless, significant displacements are likely to develop at the seismic isolation floor. To address this shortcoming, hybrid seismic isolation system have been proposed, in which isolation bearings are combined with supplemental damping devices to provide enhanced control. These systems have been extensively investigated and are acknowledged as an effective strategy for mitigating both excessive isolator displacements and superstructure demands (He et al., 2024). The smart seismic isolation (SBI) system, which combines seismic isolation and an MR a magnetorheological damper (MR damper), is an example of such hybrid techniques and has a number of benefits. It shows that it can adjust to both near-field and far-field earthquakes and offers a considerable decrease in base drift. However, a potential drawback of the SBI system is that it may increase seismic responses in the superstructure, such as inter-story drifts and story accelerations, compared to a conventional passive seismic isolation system without an MR damper (Mohebbi & Dadkhah 2019). When opposed to passive systems, well-designed active and semi-active hybrid systems may generally offer better seismic performance; however, their practical implementation may face challenges related to complexity and reliability (He et al., 2023). Regarding the operational behavior and practical considerations of hybrid systems, practically, the active component operates only under significant excitations, whereas under normal conditions the system behaves passively. If the actuator capacity is exceeded or a power outage occurs, the device automatically switches to passive mode until stable conditions are restored. Although installation costs are relatively high, the limited operation of the active part results in reduced maintenance and operating expenses compared to fully active systems.

1.1.4 Passive control systems

Passive control systems are mechanical devices designed to manage the energy imparted to a structure by dynamic loads, ensuring that the structural response does not exceed its inherent capacity. These systems dissipate incoming energy through elements placed between the structure and its foundation, converting it into heat or kinetic energy. Energy dissipation can occur through friction, plastic deformation, phase changes, or the deformation of viscoelastic solids and fluids, or alternatively, by transferring energy into vibrational modes using pendulum-like elements that act as dynamic dampers. Figure 1.2 shows the general operation of passive control systems (Constantinou et al., 1998). The fact that passive control systems don't need an external power source is one of their main benefits, which makes them a dependable and affordable option. Because of these features, passive systems are highly effective against unpredictable dynamic events such as strong winds and earthquakes. When properly designed, passive devices can control both section forces and displacements, thereby enhancing structural performance and preventing excessive deformations. Overall, passive energy dissipation systems are designed in various forms and mechanisms, with classification dependent on the specific dynamic behavior of the structure and the intended functional requirements.

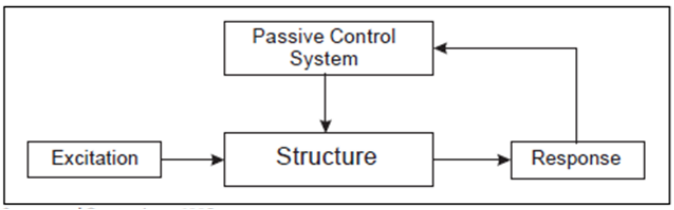

Figure 1.2 : The general working principle of passive control systems. (Constantinou et al., 1998).

In structural design, the inherent uncertainties related to seismic loads and structural characteristics are commonly acknowledged. Traditional seismic design approaches often allow inelastic deformations under extreme hazard conditions to distribute seismic energy and reduce both force demands and structural responses. However, in certain situations, permitting inelastic behavior may not be acceptable, which can limit the economic feasibility of conventional seismic design strategies. In such cases, vibration control methodologies offer a practical alternative. Among these, passive energy dissipation devices have proven to be particularly effective. Representative examples of passive control devices include friction dampers, viscous fluid dampers, seismic isolators, tuned liquid dampers, and tuned mass dampers, all of which aim to mitigate structural vibrations and enhance overall seismic performance.

1.1.5 Seismic isolation

One of the best strategies for reducing the damage that earthquakes can do to structures is seismic isolation. During seismic occurrences, this technology uses isolators to separate the structure from the base; these isolators usually provide low horizontal rigidity and high vertical stiffness. By moving the building's fundamental frequency away from its fixed-base frequency and the main frequencies of ground motion, this reduces seismic loads and structural accelerations (Sapountzakis et al., 2024). Seismic reactions in seismically isolated buildings are reduced by shifting or prolonging the building's basic natural period away from the energetic frequency range of ground motion. Earthquakes, as dynamic actions, induce significant forces on structures. In the determination of these forces, the horizontal elastic design acceleration spectrum defined in TSC (2018), as illustrated in Figure 1.3, is adopted. When generating ground motion spectra for a given earthquake, a standard damping ratio of 5% is considered. The spectra are specifically defined by accounting for local soil conditions, mapped spectral acceleration coefficients, and near-fault effects, in accordance with the provisions of TSC (2018).

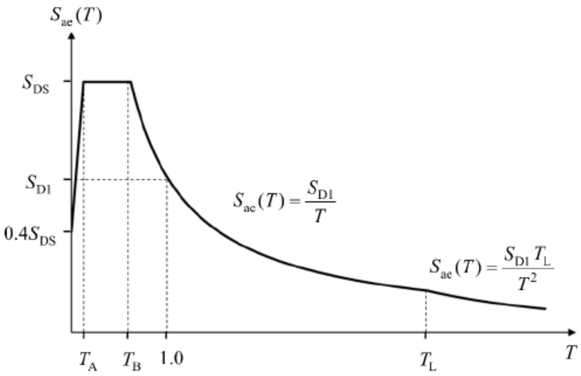

Figure 1.3 : The horizontal elastic design acceleration spectrum (TSC, 2018).

Figure 1.4 illustrates the influence of seismic isolation on the inertial forces developed in a typical structure subjected to earthquake loading. As can be seen from the period shift in Figure 1.4, the insertion of the isolation system causes the fundamental period of the structure to significantly lengthen. Seismic accelerations communicated to the superstructure are significantly reduced as a result of this extension of the natural period. In most cases, the reduction in acceleration demand exceeds a factor of three when considering a fixed-base structural system. Consequently, the corresponding inertial forces acting on the structural elements are markedly reduced. This reduction enables the economical design of structural systems that are capable of remaining within the elastic range and avoiding structural damage under design-level earthquake excitation The impact of seismic isolation on the structure's displacement response is shown in Figure 1.5. In isolated structural systems, the overall seismic displacement demand is primarily accommodated by the isolation layer. As a result, the relative displacements within the superstructure are significantly reduced. The isolation system effectively decouples the superstructure from ground motion, thereby limiting deformation demands on primary structural members. As a result, the superstructure and other structural elements sustain little harm, and the isolation mechanism dissipates most of the seismic energy.

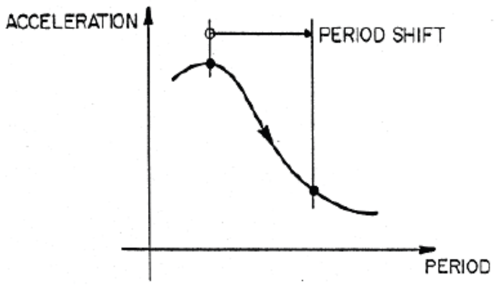

Figure 1.4 : Impact of period elongation obtained by seismic isolation on accelerations (Constantinou et al., 2007).

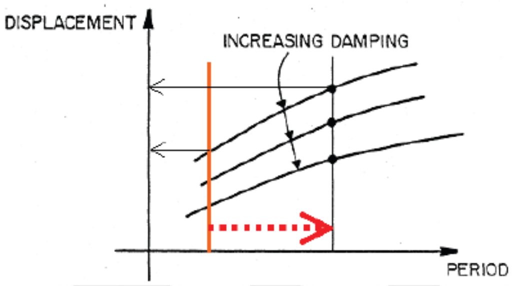

Figure 1.5 : Impact of period elongation obtained by seismic isolation on displacements (Constantinou et al., 2007).

By extending the natural period, floor accelerations are significantly reduced; however, larger displacements may occur at the isolator level and within the superstructure when observed from the displacement response spectrum perspective. The larger displacements and residual accelerations resulting from seismic isolation are controlled through the high damping capacity of the isolation system, which limits structural responses to acceptable levels in both acceleration and displacement spectrum perspectives. Potential measures to further manage excessive movements include increasing damping within the isolators or integrating high-damping devices into the isolation layer. It should be noted, however, that such modifications may also lead to increases in superstructure accelerations and inter-story drifts, necessitating careful design considerations.

According to Chen et al. (2016), traditional seismic isolation devices include elastomeric bearings, lead rubber bearings, sliding bearings, roller bearings, and a variety of other types. Reducing a building's seismic risk can now be accomplished with reliable and affordable seismic isolation devices. Within the scope of this thesis, the focus is limited to elastomeric (rubber-based) isolation systems.

1.1.5.1 Elastomeric (rubber-based) seismic isolation systems

One of the most popular seismic isolation techniques in modern structural engineering applications is elastomeric isolation systems.These systems are typically manufactured using rubber based materials. This mechanical characteristic enables the isolators to effectively support vertical loads while allowing horizontal flexibility during seismic events. The steel laminations embedded within the rubber layers play a crucial role in carrying the weight of the superstructure and preventing excessive vertical deformation. Multilayer elastomeric bearings reinforced with steel plates can be classified into three main categories based on their damping and energy dissipation characteristics: low damping rubber bearing systems (LDRB), high damping rubber bearing systems (HDRB), and lead rubber bearing systems (LRB).

Low damping rubber bearing systems (LDRB)

Low damping rubber seismic isolators are a type of bearing composed of multiple layers of natural rubber and steel plates laminated together, without the inclusion of a vertical lead core. Figure 1.6 illustrates a low-damping rubber bearing (URL-3). These bearings utilize natural rubber, which is characterized by a relatively low inherent damping capacity, typically in the range of approximately 2–3% equivalent damping. Despite the low damping ratio, natural rubber isolators exhibit excellent linear behavior and provide a stable restoring force. Since the inherent energy dissipation is limited, an additional damping device is generally required. However, this configuration offers greater flexibility in the overall seismic isolation design (URL-2).

Figure 1.6 : Low damping rubber bearing (URL-3).

High damping rubber bearing systems (HDRB)

High damping rubber bearings exhibit both elastic stiffness and inherent energy dissipation capabilities within a single isolation element. Figure 1.7 illustrates a high-damping rubber bearing (URL-4). Owing to their relatively high damping capacity, the use of an additional external damping device is generally not required, which makes these systems particularly advantageous for structures with limited space availability. Furthermore, the smooth shape of their hysteresis loops allows for an effective reduction of transmitted seismic forces, enabling seismic isolation to be extended not only to the main structural system but also to sensitive equipment located within the building (URL-2).

Figure 1.7 : High damping rubber bearing (URL-4).

Lead rubber bearing (LRB)

This type of bearing has a lead core placed in the middle of a natural rubber lamination. In this configuration, the rubber layers primarily provide the elastic stiffness required for seismic isolation, while the lead core serves as the main source of energy dissipation through yielding. Due to its inherent damping capability, the use of an additional external damping device is generally unnecessary, which makes this system particularly suitable for applications with limited available space. The hysteretic behavior of lead rubber bearings is typically characterized by an elastoplastic response (URL-2). Figure 1.8 illustrates a high-damping rubber bearing (URL-5).

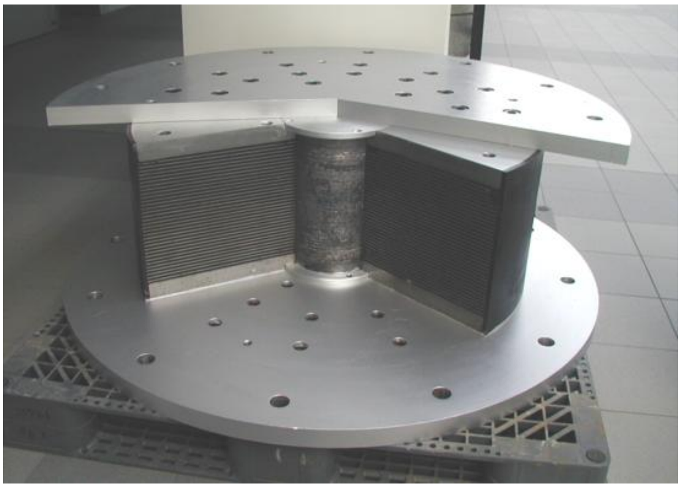

Figure 1.8 : Lead rubber bearing (URL-5).

1.2 Overview of Seismic Isolation

1.2.1 Literature review

In an effort to lessen structural susceptibility, Castillo et al. (2024) used real-time hybrid simulations to assess the seismic performance of unconnected fiber-reinforced elastomeric isolators (U-FREI) for low-rise thin reinforced concrete wall buildings. Chen et al. (2025) developed and validated an Improved Bouc-Wen model for HDRBs and compared their seismic performance with LRBs through incremental dynamic analysis. Similarly, Gowda Kiran & Noroozinejad Farsangi (2020) assessed the effectiveness of LRBs in mitigating structural responses to blast loadings on low-rise, long-span structures using adaptive modal pushover analysis, while Ibrahim (2025) investigated the seismic vulnerability of a theoretical hospital under fixed-base, soil-structure interaction, and seismically isolated scenarios, focusing on key damage indicators such as roof displacements, interstory drift ratios, and isolator displacements. Collectively, these studies demonstrate that advanced seismic isolation system effectively enhance structural dynamic performance, particularly by reducing drift and displacement.

Abrar and Tuhta (2022) investigated the performance of elastomeric seismic isolators in protecting medium-rise structures from long-period earthquakes by comparing isolators with different natural periods (2.5, 4, and 5 seconds) in mitigating earthquake energy, while Deringol and Guneyisi (2023) examined the seismic behavior of high-rise buildings equipped with LRB isolators and evaluated how adjusting the isolation period enhances seismic performance. In both studies, the use of LRB-type isolators effectively improved structural dynamic responses, particularly by reducing drift, acceleration, and shear forces.

Md et al. (2024) examined the compressive stiffness and horizontal force-displacement response of unreinforced rubber in unreinforced masonry buildings to determine how successful it is as a seismic isolator. Manchalwar & Bakre (2020) studied U-shaped steel dampers as an isolation system and compared their performance with lead rubber bearings in reducing seismic responses. To improve the seismic resistance of nuclear structures against severe earthquakes, Liu et al. (2024) suggested a hybrid multi-dimensional isolation system that combines geotechnical seismic isolation with three-dimensional seismic isolation. In five hospitals affected by the earthquakes on February 6, 2023, Kaatsız et al. (2024) assessed the seismic performance of seismic isolation systems. Baidya & Roy (2024) assessed the optimal seismic performance of a multi-storey building isolated with an SMARB device, focusing on minimizing top-story acceleration through particle swarm optimization while considering different soil types. Usta (2021) highlighted the impact of isolators on structural behavior under earthquake loads while discussing the use of seismic isolation systems utilizing finite element techniques for the seismic assessment of historic masonry buildings. Although these studies have different objectives, they consistently demonstrate improvements in building displacement and acceleration responses.

Jasim et al. (2024) investigated optimal isolator types to enhance the fundamental period and reduce base shear, top-storey displacement, and interstory drifts, including comparisons with tuned mass dampers (TMDs) and evaluation of integrated seismic isolator–TMD systems across varying building heights and earthquake intensities. Thakur & Tiwary (2023) assessed the seismic performance of hybrid structures with CFST and CES columns compared to conventional RCC structures, emphasizing the effectiveness of fluid viscous dampers and seismic isolation in mitigating seismic responses and enhancing building resilience. Hu (2014) examined the advantages of LRB isolation in steel frame buildings subjected to near-fault ground motions, focusing on base shear and interstory drift performance. Madhukumar et al. (2022) analyzed the performance of seismic isolation using LRBs in multi-storey RC framed structures of varying heights through response spectrum and pushover analyses. All of these investigations show that structural drift and shear force responses can be effectively improved by using hybrid damping systems and seismic isolation.

The performance of the seismic isolation system and the building's long-term seismic response characteristics were the main topics of Siringoringo & Fujino's (2014) analysis of the seismic reaction of a seismically isolated building during the 2011 Great East Japan Earthquake. The study found that the building experienced a reduction in frequency and increased damping during the main shock.

Ziraoui et al. (2024) evaluated the effectiveness of seismic isolation system using LRBs in reducing seismic responses of multi-storey reinforced concrete buildings, observing improvements in moment, displacement, and interstory drift. Ye & Nyangi (2021) enhanced the seismic performance of dual-isolated structures by incorporating supplemental inerters to control relative displacements, reporting improvements in displacement, acceleration, and moment responses. Kumar & Saha (2021) investigated the seismic performance of elevated liquid storage tanks, considering soil-structure interaction, tank slenderness, staging stiffness, and isolator period, and observed positive effects on moment and shear force responses with seismic isolation. Manna et al. (2024) assessed the effectiveness of seismic isolation in protecting buildings with secondary structures under earthquakes and pulse-type ground motions, showing improvements in moment, shear force, and drift. Nasery et al. (2015) examined seismic isolation in a high-ductility hospital-type structure, highlighting enhancements in moment, displacement, and shear force. Finally, Sugihardjo & Lesmana (2019) studied the seismic response of residential buildings equipped with perforated-reinforced elastomeric isolators (PREIs) under strong ground motions in Indonesia, reporting improvements in acceleration, shear force, and moment. Collectively, these studies demonstrate that seismic isolation system significantly enhance structural dynamic responses, particularly in terms of moment, displacement, drift, shear force, and acceleration.

Ozer and Inel (2025) compared fluid viscous dampers, LRBs, and friction pendulum sliders to fixed-base models on a mid-rise reinforced concrete structure with torsional irregularity. A seismic isolation system that combines friction pendulum isolators with a Tuned Fluid Inerter (TFI) was proposed by De Domenico et al. (2020), demonstrating decreased displacement, acceleration, and interstory drift. Shang et al. (2021) investigated a variable friction pendulum bearing (VFPB) and developed a design approach, comparing it with conventional FPBs. Deringol & Guneyisi (2021) applied HDRBs to steel buildings and designed a compact intelligent isolation system. All studies reported improvements in structural drift and acceleration responses.

Yuan et al. (2025) optimized a rubber bearing isolation scheme for the Dong Wind and Rain Bridge to balance safety and heritage preservation. Sulthan & Seki (2023) analyzed seismically isolated buildings in Indonesia and conducted seismic fragility assessments. Domadzra et al. (2024) studied the effects of LRB and FPS-bearing properties on seismically isolated buildings. Baidya & Roy (2023) compared SMA materials in seismic isolation system, optimizing top-floor acceleration using particle swarm optimization. Lo Frano (2018) evaluated seismic isolation benefits for nuclear structures, particularly SMRs. Falborski & Jankowski (2017) experimentally verified a polymeric bearing prototype for vibration reduction. All studies reported improved structural acceleration performance.

Lai et al. (2025) developed and assessed a double-sided sliding horizontal-vertical decoupling seismic isolation bearing (DS-HVDB) to enhance seismic isolation performance and mitigate torsional effects through shaking table experiments. In order to achieve seismic resilience, Babu & Zubedi (2019) stressed the importance of seismic isolation and taking soil-structure interaction into account. Saritas et al. (2022) implemented LRBs to improve the seismic performance of a high-rise building exhibiting torsional instability. Ozer & Inel (2021) investigated the influence of different LRB and FPS isolator configurations on the seismic response of a typical reinforced concrete residential building. Overall, these studies consistently demonstrate improvements in shear and torsional responses.

Ganji & Kazem (2017) examined lateral displacement and shear force distribution while comparing the seismic performance of steel structures fitted with LRBs or viscous dampers during near-field earthquakes. Chanda & Debbarma (2020) developed fragility curves for a six-storey RC seismically isolated building using LRBs and incremental dynamic analysis. Agrawal, Verma, & Kumar (2025) compared LRB and FPB performance in an eight-storey RC building in terms of displacement, fundamental period, and base shear. Islam & Al Kutti (2018) examined the effects of LRB-based seismic isolation on multistory buildings, assessing changes in lateral forces, displacement, inertia, and story accelerations. By analyzing several isolation systems and their effects on seismic performance, Ashokkumar et al. (2025) offered recommendations for the best location of dampers in medium- and high-rise buildings. Habib et al. (2021) investigated the time-history response of irregular seismically isolated RC structures under near-fault pulse-like earthquakes, considering isolator damping ratios and structural irregularities. Collectively, these studies report significant improvements in structural shear force responses.

Ozer, Inel, and Cayci (2022) examined behavioral variations and nonlinear effects while comparing the seismic responses of fixed-base and seismically isolated models (LRB, FPS, and FS) for typical low- and mid-rise RC buildings. It was observed that while seismically isolated models exhibit higher total lateral displacements, these demands are substantially reduced at the isolator interface.

1.2.2 Purpose of the thesis

The inherent uncertainty of earthquakes has always posed significant challenges for humanity. In this context, ensuring the seismic resilience of inhabited structures is of paramount importance, as the performance of buildings plays a critical role in mitigating earthquake-induced risks. In Turkey, and particularly in the megacity of Istanbul, earthquakes represent a constant and unpredictable threat due to high seismicity and dense urban development.

The main objective of this thesis is to investigate the seismic performance of a residential reinforced concrete building located in Istanbul and to evaluate the effectiveness of seismic isolation systems in enhancing its structural behavior under earthquake loading. For this purpose, the selected building is retrofitted using two different seismic isolation systems: lead rubber bearings (LRB) and high-damping rubber bearings (HDRB). The fixed-base and base-isolated configurations seismic responses are compared, with a focus on enhancements to structural safety and functional performance.

In addition to the reference structural configuration, an alternative modeling approach with reduced material strength is also considered to represent the characteristics of existing reinforced concrete building stock. This allows for the evaluation of seismic isolation performance not only for newly designed structures but also for existing buildings constructed with lower material quality. By considering both material scenarios, the study seeks to provide additional insight into the influence of material degradation on the seismic response of isolated structures and to contribute to the understanding of the potential role of seismic isolation systems in lowering seismic demands in existing urban buildings.

2. DESIGN OF BUILDINGS WITH SEISMIC ISOLATION ACCORDING TO TSC-2018

2.1 Fundamental Principles of Design

The design principles for seismically isolated buildings in Türkiye are defined in Chapter 14 of TSC-2018, effective from January 1, 2019. This section summarizes the key provisions of the code related to seismic isolation, emphasizing the design approach, analysis requirements, and performance objectives defined in the regulation. The current regulation introduces specific classifications for different earthquake levels. According to TSC-2018, the design is based on both DD-2 (design earthquake ground motion) and DD-1 (maximum considered earthquake ground motion) levels, as outlined in Table 2.1. For the DD-1 level, the lower bound values of the isolation system parameters are used, whereas for the DD-2 level, the upper bound values are considered.

Table 2.1 : Earthquake ground motion levels (TSC,2018).

Earthquake Levels	Characteristic	Probability	Recurrence Period
DD-1	Very Infrequent	2%	2475
DD-2	Rare	10%	475
DD-3	Frequent	50%	72
DD-4	Very Frequent	68%	43

According to TSC-2018, for buildings incorporating seismic isolation, the Building Importance Factor (I) shall be taken as 1. In the structural analysis model, isolation system must be modeled to reflect their nonlinear behavior. For the superstructure, the effective section stiffness factors for columns and beams are determined according to the ductility level.

2.2 Load Combinations

The load combinations specified in equation 2.1, equation 2.2, and equation 2.3 are considered for assessing the loads transferred to the structural elements beneath the isolation interface.

$$1.4G + 1.6Q \quad (2.1)$$

$$1.2G + Q \pm E_d \quad (2.2)$$

$$0.9G \pm E_d \quad (2.3)$$

The load combinations incorporating seismic effects for the superstructure design are presented in TSC 2018 Section 4.4.4, while those to be used as the basis for the design of structural system elements are defined in equation 2.4 and equation 2.5.

$$G + Q + 0.2S + E_d^{(H)} + 0.3E_d^{(z)} \quad (2.4)$$

$$0.9G + H + E_d^{(H)} - 0.3E_d^{(z)} \quad (2.5)$$

The dead load effect is represented by G, the live load effect by Q, the snow load effect by S, and the horizontal ground pressure by H. The horizontal seismic effect is represented by E_d^H, while the vertical seismic effect is represented by E_d^Z. In determining the loads to be applied in the testing of isolation system, the load combinations defined in equation 2.6 to equation 2.7 are considered.

$$1.4G + 1.6Q \quad (2.6)$$

$$0.9G \pm E_d \quad (2.7)$$

2.3 Design Principles of the Isolation System

2.3.1 Elastomeric isolation system

Given its nonlinear behavior in the time domain, the isolation system must have enough capacity to handle the displacements and axial forces obtained for the isolation system under the DD-1 earthquake ground motion. Variations in the isolation system parameters caused by axial force, temperature, rate effects, and similar variables are included in the design unless experimental data indicates otherwise.

2.3.2 Lower and upper bound values to be used in design

The nominal values are multiplied by the factors λ_{upper} and λ_{lower}, respectively, to yield the upper and lower bound values of the isolation system parameters utilized in the computations. The λ_{upper} and λ_{lower} values are calculated using the expressions given in equation 2.8 and equation 2.9.

$$\lambda_{upper} = [1 + 0.75(\lambda_{ae,upper} - 1)]\lambda_{test,upper}\lambda_{spec,upper} \tag{2.8}$$

$$\lambda_{lower} = [1 - 0.75(1 - \lambda_{ae,lower})]\lambda_{test,lower}\lambda_{spec,lower} \tag{2.9}$$

When λ_{upper} or λ_{lower} values cannot be obtained from prototype or production control tests, the corresponding lower and upper bound values given in Table 2.2 are adopted in the calculations. In Table 2.2, KCE refers to the LRB system, and YSE refers to the high-damping elastomer system. F_Q stands for the lead-rubber bearing's characteristic strength, and k_2 for its post-elastic stiffness. Aging and environmental impacts, testing conditions, and manufacturing variability are taken into consideration by the parameters λ_{ae}, λ_{test}, and λ_{spec}, respectively.

Table 2.2 : Recommended lower and upper bound values of strength and stiffness parameters for elastomeric isolation system (TSC, 2018).

Parameter	Type	F_Q		k_2	
		Lower	Upper	Lower	Upper
$\lambda_{æ}$	KCE	1.00	1.10	1.00	1.30
	YSE	1.00	1.30	1.00	1.40
λ_{test}	KCE	0.70	1.30	0.90	1.30
	YSE	0.70	1.30	0.90	1.30
λ_{spec}	KCE	0.85	1.15	0.85	1.15
	YSE	0.85	1.15	0.85	1.15

2.3.3 Unit deformation limits of elastomeric isolation system

The components of unit deformation occurring under non-seismic conditions are given in equation 2.10, equation 2.11, and equation 2.12.

(a) Angular deformation due to compression :

$$\gamma_{c,st} = \frac{6SP_{K1}}{A_r E_c} \tag{2.10}$$

Here, P_{K1} represents the vertical force under the load combination specified in equation 2.1, and A_r is the area of a single elastomer layer bonded to steel plates and subjected to load. S represents the shape factor and E_c is the compressive modulus of the elastomeric isolation system.

(b) Angular deformation due to horizontal displacement from non-seismic effects (expansion, wind, etc.) :

$$\gamma_{s,st} = \frac{\Delta_s}{T_r} \tag{2.11}$$

Here, Δ_s is the horizontal displacement resulting from horizontal loading, and T_r is the total thickness of the elastomer layers.

(c) Unit deformation brought on by the isolation system's upper and lower plates rotating relative to one another :

$$\gamma_{r,st} = \frac{B^2 \theta_S}{2tT_r} \tag{2.12}$$

The design rotation angle, θ_s, includes the rotational effects due to dead loads, live loads, and manufacturing processes. A minimum value of 0.005 radians is considered. In this context, B denotes the diameter of the elastomer bonded to the steel plate, t represents the thickness of an individual elastomer layer, and T_r is the total thickness of the elastomer.

According to TSC 2018, the unit deformations developing in the elastomer material under DD-1 and DD-2 earthquake ground motion levels, considering seismic and vertical load effects, shall be calculated as defined below in (a) and (b) (TSC, 2018).

(a) The unit deformation due to compression under DD-1 and DD-2 earthquake ground motions shall be calculated using the following equation 2.13 :

where the vertical force derived under the load combination specified in equation 2.2 is denoted by P_{K2}.

$$\gamma_{c,E} = \frac{6SP_{K2}}{A_{rc}E_c} \tag{2.13}$$

(b) Equation 2.14 must be used to get the unit deformation resulting from horizontal displacement under DD-1 and DD-2 earthquake ground motions.:

$$\gamma_{s,E} = \frac{D}{T_r} \tag{2.14}$$

The unit deformations in the elastomeric isolation system are expected to meet the following conditions (TSC, 2018).

(a) The unit deformations in the elastomer material due to vertical loads, excluding seismic effects, are required to satisfy the smaller of the limits given in equation 2.15 and equation 2.16. In these equations, ε_b denotes the failure strain of the elastomer material.

$$\gamma_{c,st} \leq 3.5 \text{ or } \gamma_{c,st} < \varepsilon_b/3 \tag{2.15}$$

$$\gamma_{c,st} + \gamma_{s,st} + \gamma_{r,st} \leq 5.0 \text{ or } \gamma_{c,st} + \gamma_{s,st} + \gamma_{r,st} < 0{,}75\varepsilon_b \tag{2.16}$$

(b) The total unit deformation at the elastomer material interface, resulting from horizontal displacement and rotation, is required to satisfy the limits given in equation 2.17 and equation 2.18.

$$\gamma_{c,E} + \gamma_{s,E} + 0.5\gamma_{r,st} \leq 6.0 \tag{2.17}$$

$$\gamma_{s,E} \leq 2.0 \tag{2.18}$$

2.3.4 Vertical stability of elastomeric isolation system

In the absence of horizontal displacement, the buckling load P_{cr} of elastomeric isolation system is determined using equation 2.19 for circular-section units without a lead core, equation 2.20 for square-section units without a lead core, and equation 2.21 for lead-rubber bearing units.

$$P_{cr} = \frac{0.218 G_v B^4}{t T_r} \tag{2.19}$$

$$P_{cr} = \frac{0.340 G_v B^4}{t T_r} \tag{2.20}$$

$$P_{cr} = 0.218 \frac{G_v B^4}{t T_r} \frac{(1 - B_L/B)(1 - B_L^2/B^2)}{1 + B_L^2/B^2} \tag{2.21}$$

B_L stands for the lead core's diameter, and G_v for the elastomer material's shear modulus. When horizontal displacement occurs, the buckling load P_{cr} of elastomeric isolation system under the DD-1 earthquake ground motion is calculated using equation 2.22.

$$P_{cr} = P_{cr}(A_{ro}/A) \tag{2.22}$$

Ar is determined using the following expressions, as illustrated in Figure 2.1. For the value of D, D_{TM} is applied (TSC, 2018).

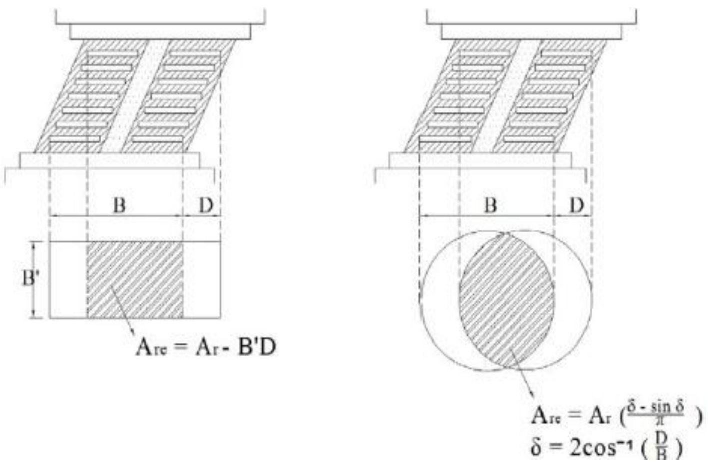

Figure 2.1 : Parameters used in the calculation A_{re} (TSC,2018).

The axial load capacity of elastomeric isolation system, as a function of unit deformation, is calculated using equation 2.23.

$$P_{str} = \frac{3.5 A_{ro} E_c}{6S} \tag{2.23}$$

The buckling load limit of elastomeric isolation system in the absence of horizontal displacement is given by equation 2.24.

$$\frac{\min(\mathrm{P_{cr}}, \mathrm{P_{str}})}{\mathrm{P_{K1}}} \geq 2.0 \qquad (2.24)$$

The buckling load limit of elastomeric isolation system under the horizontal displacement occurring at the maximum earthquake ground motion level is given by equation 2.25.

$$\frac{min(P'_{cr}, P_{str})}{P_{K2}} \geq 1.1 \qquad (2.25)$$

2.3.5 Fundamental characteristics of elastomeric isolation system

Figure 2.2 illustrates elastomeric isolator units composed of alternating layers of steel plates and natural rubber (or neoprene), which work together to provide vertical load-bearing capacity while allowing horizontal flexibility for seismic isolation purposes (TSC, 2018).

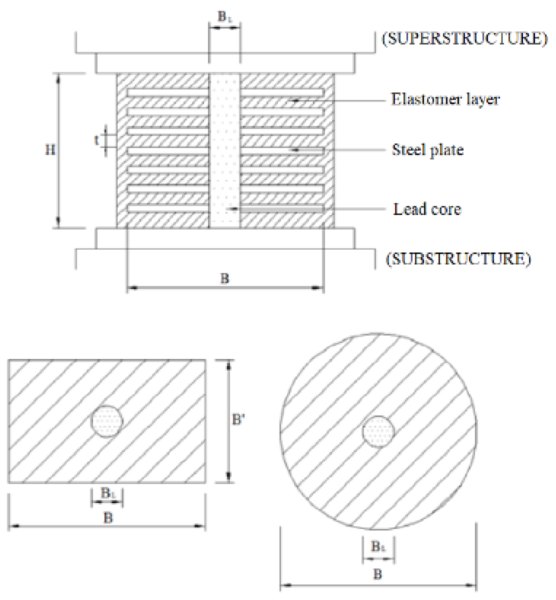

Figure 2.2 : Elastomeric isolator units composed of alternating layers of steel and natural rubber (or neoprene) plates (TSC, 2018).

Figure 2.3 illustrates a simplified force–displacement (loading cycle) curve of the isolation system, representing the characteristic hysteretic behavior of the isolator under cyclic loading conditions (TSC, 2018).

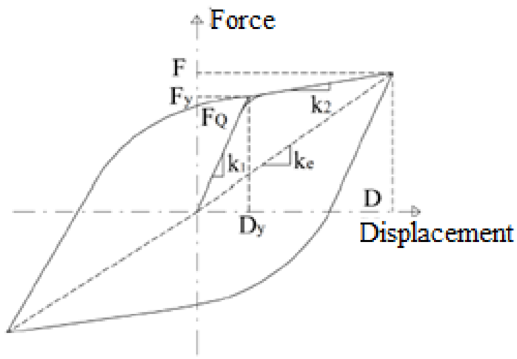

Figure 2.3 : Simplified force–displacement (loading cycle) curve of the isolation system (TSC, 2018).

In this case, k_1 stands for the initial (elastic) stiffness, k_2 for the secondary (post-elastic) stiffness, and F_Q for the characteristic strength. The horizontal force at displacement D is represented by F in equation 2.26, which also shows the effective stiffness corresponding to the displacement D. The effective yield strength and effective yield displacement are indicated by F_y and D_y, respectively.

$$k_e = \frac{F}{D} \tag{2.26}$$

The effective damping ratio, β_e, is determined using equation 2.27, where W_d represents the energy dissipated during a loading cycle.

$$\beta_e = \frac{1}{2\pi}[\frac{W_d}{FD}] \tag{2.27}$$

Equation 2.28 is used to get the characteristic strength F_Q of a lead-rubber bearing.

$$F_Q \cong F_y = A_p \tau_{yp} \tag{2.28}$$

The elastic stiffness of the lead core determines the initial stiffness of a lead-rubber bearing. Equation 2.29 is used to determine the elastomeric isolation system's secondary (post-elastic) stiffness.

$$k_2 = G_V (A_r / T_r) \tag{2.29}$$

The area A_r for circular-section lead-rubber bearings is determined using equation 2.30, while for rectangular-section lead-rubber bearings, it is determined using equation 2.31.

$$A_r = (\pi/4)(B^2 - B_L^2) \tag{2.30}$$

$$A_r = BB' - (\pi B_L^2/4) \tag{2.31}$$

The elastomeric isolation system's form factor S is calculated by dividing the loaded surface area. Equation 2.32 expresses the A_r of each elastomer layer attached to a steel plate by the lateral surface area of the elastomer layer A_L.

$$S = A_r / A_L \tag{2.32}$$

Equation 2.33 is used to get the value of S for circular-section lead-rubber bearings. In this case, B stands for the diameter of the elastomer layer bonded to the steel plate, BL for the diameter of the lead core, and t for the elastomer layer's thickness.

$$S = (B^2 - B_L^2)/(4Bt) \tag{2.33}$$

Equation 2.34 is used to compute the elastomeric isolation system's vertical stiffness, kv.

$$k_v = \frac{E_v A_r}{T_r} \tag{2.34}$$

The vertical stiffness modulus E_V in equation 2.34 is calculated using equation 2.35.

$$E_v = \frac{1}{\frac{1}{E_c} + \frac{1}{K}} \tag{2.35}$$

Here, K is the rubber material's bulk modulus, which is assumed to be 2000 MPa, and Ec is the elastomeric isolation system's compressive modulus, which is computed using equation 2.36.

$$E_c = E_0(1 + 2kS^2) \tag{2.36}$$

The rubber material's elastic modulus, E0, is determined by the formula E0 = 4Gv. For rubber hardness levels of 50, 60, and 70, the coefficient k is assumed to be 0.75, 0.60, and 0.55, respectively.

3. NUMERICAL EXAMPLE

This section provides a detailed description of the analyses conducted as part of the thesis. Firstly, the modeling of the buildings and structural systems, the mechanical properties and dimensions of the isolators used in the seismic isolation system, and the earthquake records used in the time-history analysis are presented.

The study focuses on the numerical modeling of a seven-story residential–commercial reinforced concrete structure utilizing lead rubber bearing isolation and high damping rubber bearing isolation systems. To compare the seismic performance of seismic isolators, the cases where the building base is fixed and the seismic isolator is used in both models were examined. Structure-soil interaction was ignored in the study. Time-history analysis was performed. Two different earthquake records were used for these analyses. All analyses, using structural modeling and earthquake records, were conducted using SAP2000. The structural system and loadings of conventional models were taken as reference from master's thesis titled "Earthquake Performance and Project Budget Comparison of a Conventional Building and a Seismically Isolated Building" (Catlioglu, 2021).

3.1 Modelling

The model, created using the SAP2000 software, represents a reinforced concrete building designed for residential-commercial use and consists of 7 stories. The structural system comprises columns, beams, and a two-way ribbed slab system. The most efficient way to transfer the inertia forces produced by the distributed masses on the slabs to the vertical load-bearing parts is to arrange the structural system symmetrically and regularly in plan (TSC, 2018). With a symmetrical structural layout, eccentricities arising from mass, stiffness, and strength irregularities can be minimized, allowing for a predictable seismic response.
As a result, the structure has three 4-meter-wide spans in both the X and Y axes. Additionally, the structural system's vertical arrangement should be regular, as stressed in TSC 2018. In this situation, abrupt shifts in the strength and stiffness of the tale should be avoided as much as

possible because they may result in weak or soft story constructions. In the building modeled for this thesis, no discontinuities exist between floors.

3.1.1 Material properties

In Turkey, reinforced concrete buildings make up the majority of the country's building stock. Therefore, the modeled building is considered as reinforced concrete. The use of concrete with a class lower than C25 cannot be used (TSC, 2018). For this study, C30 concrete is selected for the structural design. The concrete has a modulus of elasticity of 32.000 MPa, a characteristic compressive strength of 30 MPa, an equivalent cube compressive strength of 37 MPa, a Poisson's ratio of 0.2, a coefficient of thermal expansion of 10^{-5} /°C, and a characteristic axial tensile strength of 1.9 Mpa (TS 500, 2000). The reinforcing steel is selected as B420C, with a modulus of elasticity of 2×10^5 MPa, a minimum yield strength of 420 N/mm², a tensile strength of 500 N/mm², a Poisson's ratio of 0.30, and a coefficient of thermal expansion of 10^{-1}/°C (TS 708, 2010).

In addition to the reference material configuration, a reduced material strength scenario was also defined to represent the characteristics of existing reinforced concrete building stock. For this purpose, C15 concrete and BC1 reinforcing steel were adopted in the numerical model. BC1 reinforcing steel, representing smooth (plain) reinforcing bars commonly found in the existing building stock, was adopted to realistically reflect the material characteristics of older reinforced concrete structures. The C15 concrete was defined with a characteristic compressive strength of 15 MPa, an equivalent cube compressive strength of 18 MPa, and a reduced modulus of elasticity consistent with lower-strength concrete behavior. The reinforcing steel was modeled as BC1, representing older-generation reinforcement commonly found in existing structures. The steel was assigned a modulus of elasticity of 2×10^5 MPa, a reduced yield strength of 220 N/mm², and a corresponding tensile strength consistent with this steel class. This reduced material configuration enables the evaluation of seismic isolation effectiveness under degraded material conditions, providing a more realistic representation of the seismic behavior of existing reinforced concrete buildings.

3.1.2 Identification of structural system elements

As stated in TSC 2018, the minimum cross-section of square columns should be 30×30 cm, and the minimum beam cross-section should be 30 cm in width and 50 cm in height. In the model developed for this thesis, the column dimensions are 60 × 60 cm and the beam cross-sections are 40×60 cm. In the SAP2000 model, the beams and columns are represented as frame(bar) elements. The reinforced concrete slab, which acts in two directions, is modeled as a rigid diaphragm to ensure that all floor slabs on the same level move together. The slab thickness is taken as 15 cm. Since the foundation design is not considered in this study, the base of the structure is assigned as fixed supports. The same slab, column and beam dimensions and reinforcement details were used in all models to ensure more accurate comparisons.The effective stiffness modification factors required for reinforced concrete structural elements, as specified in TSC 2018, are given in Table 3.1.

Table 3.1 : Effective section stiffness modification factors (TSC, 2018).

Reinforced Concrete Structural Element	**Effective Section**	**Stiffness Factor**
Shear Wall–Slab (In-Plane)	**Axial**	**Sliding**
Shear Wall	0.5	0.5
Basement Shear Wall	0.8	0.5
Slab	0.25	0.25
Shear Wall–Slab (Out-of-Plane)	**Bending**	**Shear**
Shear Wall	0.25	1
Basement Shear Wall	0.5	1
Slab	0.25	1
Frame (Bar) Element	**Bending**	**Shear**
Link Beam	0.15	1
Frame Beam	0.35	1
Frame Column	0.7	1
Shear Wall (Equivalent Bar)	0.5	0.5

The modeling view of the structure is presented in Figure 3.1.

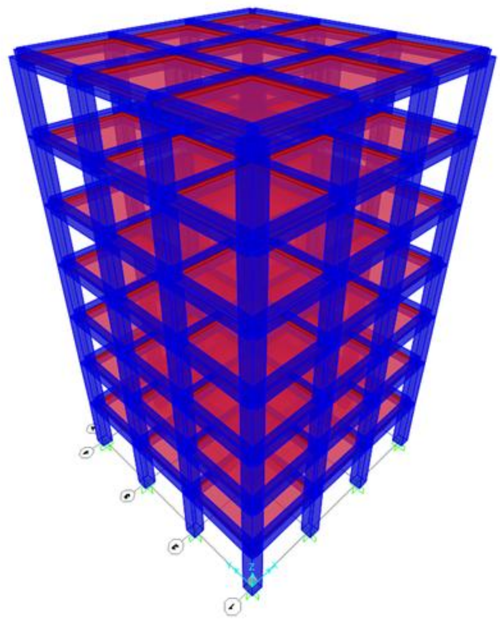

Figure 3.1 : Structural model of the building.

According to the Turkish Seismic Code, the design of buildings with seismic isolation is based on the DD-2 earthquake ground motion level (TSC 2018). The target performance levels defined for this ground motion are presented in Table 3.2. In this table, KK refers to Immediate Occupancy (IO), SH refers to Limited Damage (LD), and DGT refers to Nonlinear Time History Analysis. In this study, the target performance level under the DD-2 earthquake ground motion is selected as Immediate Occupancy (IO).

Table 3.2 : Performance targets and applicable evaluation/design approaches for seismically isolated buildings according to seismic design categories (TSC, 2018).

Earthquake Ground Motion Level	DTS =1,2,3,3a,4,4a		DTS =1a, 2a	
	Standard Performance Target	Evaluation / Design Approach	Advanced Performance Target	Evaluation / Design Approach
DD-2	SH	DGT	KK	DGT
DD-1	-	-	-	-

For the selected performance target, the earthquake load reduction factor (R) and the overstrength factor (D) defined in TSC 2018 are presented in Table 3.3. For the immediate occupancy (KK) performance target, the R factor is taken as 1.2 and the D factor is taken as 1.2.

Table 3.3 : Earthquake load reduction and overstrength factors (TSC, 2018).

Performance Target	R	D
KK	1.2	1.2
SH	1.5	1.5

According to TSC 2018, the building's use determines the building usage class (BKS) as Class 3, and the important factor (I) is set at 1.0.

Table 3.4 : Earthquake load reduction and overstrength factors (TSC, 2018).

Building Usage Class	Building Usage Description	Importance Factor (I)
BKS=1	Buildings required to remain operational after an earthquake, buildings with long-term and intensive occupancy, buildings used for storing valuable goods, and buildings containing hazardous materials	1.5
BKS=2	Buildings with short-term and intensive occupancy (shopping malls, sports facilities, cinemas, theaters, concert halls, places of worship, etc.	1.2
BKS=3	Other buildings (residential buildings, offices, hotels, industrial buildings, etc.)	1.0

3.1.3 Load combinations

Loads like dead and live loads, snow loads, earthquake loads, wind loads, and soil pressure are applied to the building's structural components. Structural elements exposed to these loads undergo deformation and displacement. The structure must provide adequate resistance against these internal forces and resulting displacements. Load combinations are established in accordance with TSC 2018 by considering dead loads, live loads, and earthquake loads together.

For the commercial-residential type models, the uniformly distributed live load (Q) is taken as 2 kN/m² (TS 498, 1987). The exterior walls of the models are considered as walls, with a wall load (Gwall) of 5 kN/m². The finishing and plaster load on the slab (Gplaster) is taken as 1.5 kN/m². In addition, the live load participation factor for commercial-residential buildings is defined as n = 0.3 according to TSC 2018.

3.1.4 Processing and preparation of strong ground motion records for structure analysis

Turkey has many active fault zones and is situated in an area with a high degree of seismic hazard because of the interaction of several tectonic plates. A significant portion of the large and destructive earthquakes recorded throughout history has occurred along these fault systems. For the structural model assumed to be located in the Bahçelievler district of Istanbul, local soil conditions were evaluated based on the study entitled “Geology of the Istanbul Provincial Area” published by the Istanbul Metropolitan Municipality (IMM) Department of Earthquake and Ground Research (IMM, 2011). According to this reference, the average shear-wave velocity of the site (V_{S30}) is approximately in the range of 350–400 m/s; therefore, in accordance with the soil classification criteria defined in TSC 2018, the site was classified as soil class ZC. Based on this soil classification, earthquake records were selected in accordance with the shear-wave velocity limits defined for the ZC soil class. A user-defined target spectrum was used to retrieve the chosen ground motion records from the PEER NGA-West2 database. The PEER earthquake database provides acceleration records in two mutually perpendicular horizontal components. In this study, these components are assigned to the global X and Y directions of the structural model. This variation results from the orientation of the seismic sensors at the recording stations and the specific configuration of each earthquake measurement. In this thesis, the available horizontal components are used as provided, allowing the structural response along different axes to be accurately evaluated. Since the reaction of buildings is mostly affected by horizontal ground vibrations, the vertical (up) component is excluded. Since the fault segments in Istanbul predominantly exhibit strike-slip behavior, particular attention was paid to selecting earthquake records with strike-slip fault mechanisms. Moreover, considering that the expected earthquake magnitude in the region is within the range of Mw = 7.0–8.0, the selected records were limited to this magnitude interval. Accordingly, the strong ground motion records RSN 864 and RSN 1166, corresponding to the 1992 Landers Earthquake (Mw = 7.3) and the 1999 Kocaeli (Izmit) Earthquake (Mw = 7.4), respectively, were used in the analyses to investigate the effects of large-scale strike-slip ground motions on structural behavior. These records were selected due to their reliable measurement quality and their capability to represent near-fault characteristics.

The Kocaeli Earthquake, RSN 1166, has a total recording duration of 29.99 seconds. The acceleration record for this earthquake, which occurred near İzmit on August 17, 1999, consists of 6.000 data points with a time step (Δt) of 0.005 seconds. As the earthquake data were provided by PEER in a processed format, no further filtering or modification was necessary. The absolute peak acceleration of the Kocaeli Earthquake in the x direction was 0.124 g, observed at 11.61 s. In the y direction, a peak acceleration of 0.0907 g was observed at 12.83 s. The acceleration-time graph of the Kocaeli Earthquake is presented in Figure 3.2.

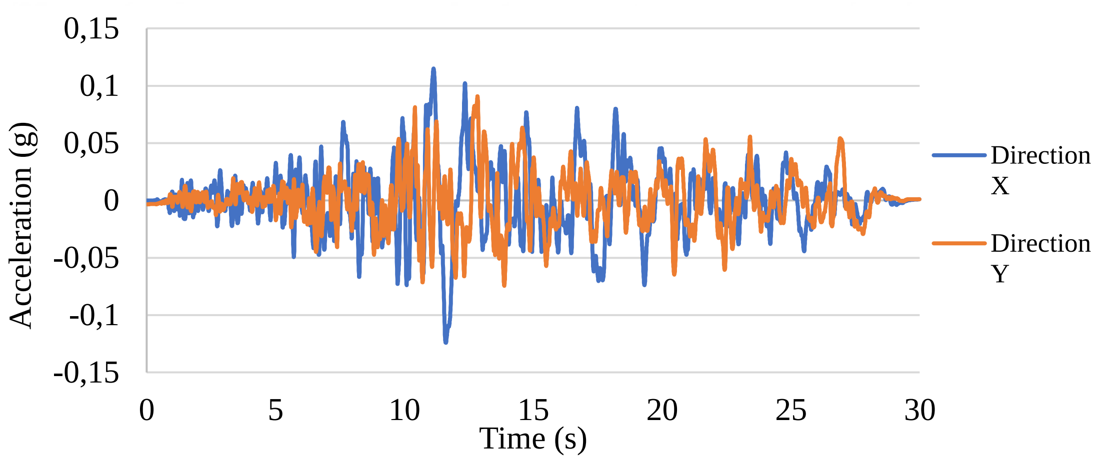

Figure 3.2 : Acceleration–time plot of earthquake record RSN 1166 (Kocaeli).

The velocity-time graph of the Kocaeli Earthquake was examined for the x direction, and the peak velocity of 25.25 cm/s was observed at 12.08 s. For the y direction, the maximum velocity of 17.30 cm/s occurred at 12.595 s. The velocity-time graph of the Kocaeli Earthquake is shown in Figure 3.3.

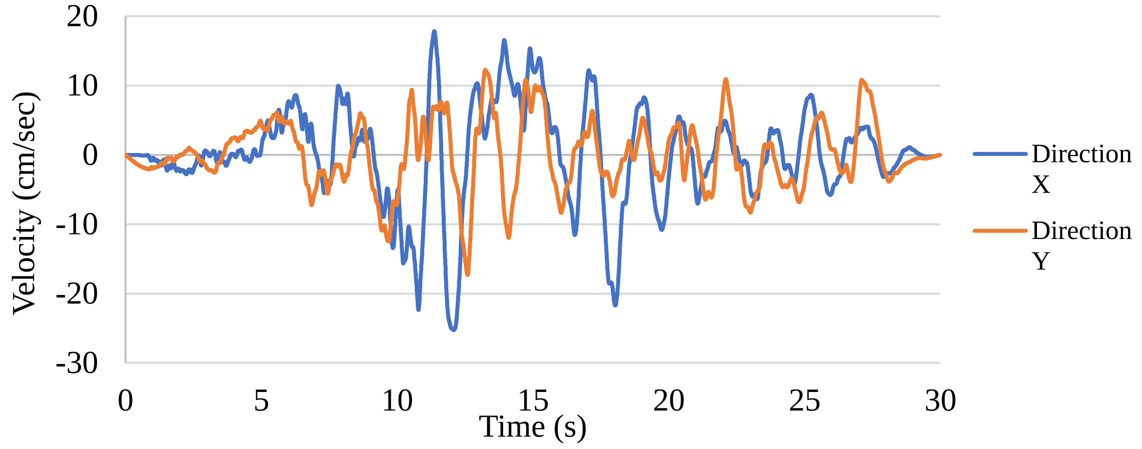

Figure 3.3 : Velocity–time plot of earthquake record RSN 1166 (Kocaeli).

The displacement-time graph of the Kocaeli Earthquake was examined for the x direction, and the peak displacement of 18.57 cm was observed at 12.58 s. For the y direction, a displacement of 6.66 cm occurred at 6.54 s. Figure 3.4 displays the displacement-time graph of the Kocaeli Earthquake.

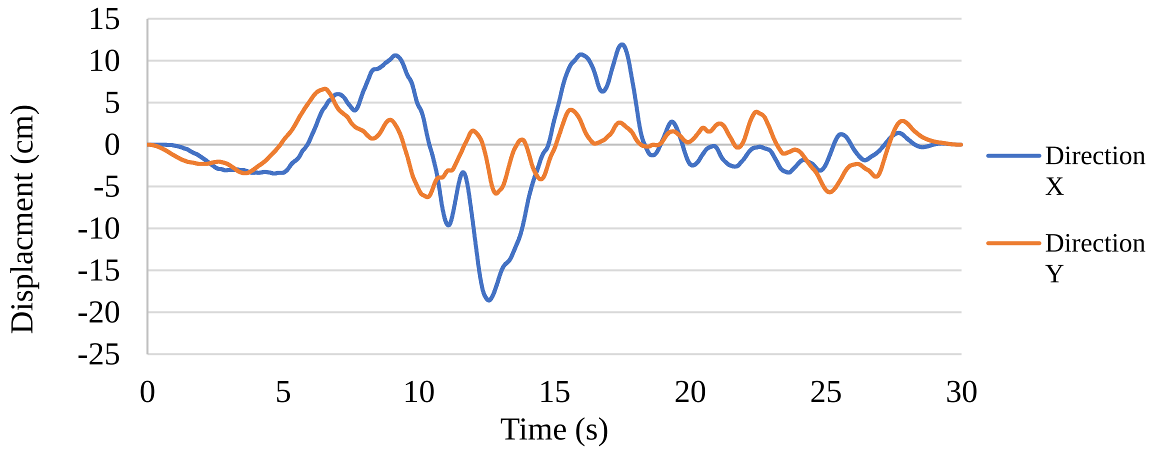

Figure 3.4 : Displacement–time plot of earthquake record RSN 1166 (Kocaeli).

The second earthquake considered in this thesis is the June 28, 1992 Landers–Joshua Tree Earthquake. Since the earthquake data were obtained from PEER as processed records, no additional filtering was applied. The earthquake record consists of 2200 data points and has a total duration of 43.96 seconds. The time step between successive points (Δt) is 0.02 s. The acceleration, velocity, and displacement time histories of the Landers–Joshua Tree earthquake are presented in Figures 3.5 to 3.7 in a respective way. The absolute peak acceleration of the Landers Earthquake in the x direction was 0.274 g, observed at 25.98 s. In the y direction, a peak acceleration of 0.284 g was observed at 9.78 s. Figure 3.5 shows the Landers Earthquake's acceleration-time graph.

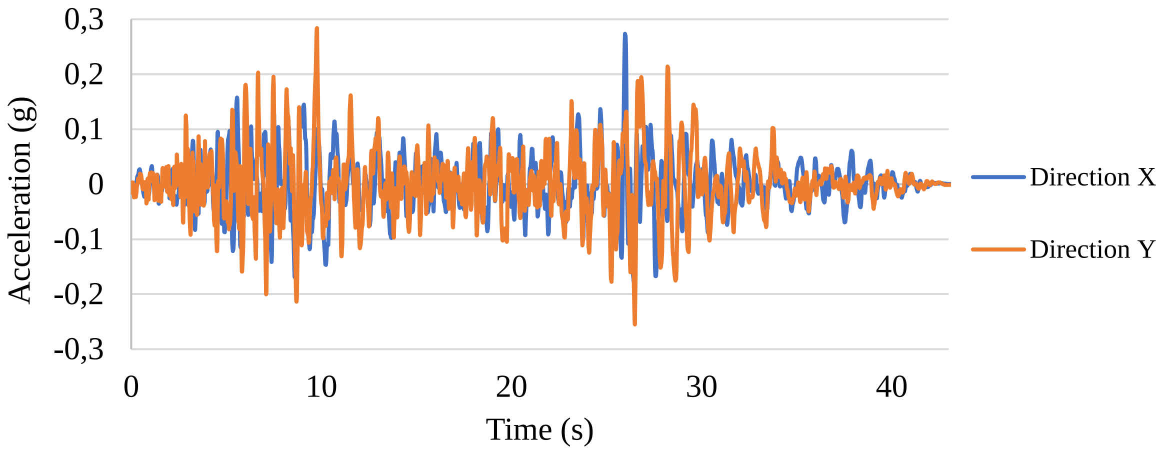

Figure 3.5 : Acceleration–time plot of earthquake record RSN 864 (Landers).

The velocity-time graph of the Landers Earthquake was examined for the x direction, and the peak velocity of 27.02 cm/s was observed at 27.48 s. For the y direction, the maximum velocity of 42.59 cm/s occurred at 26,60 s. The velocity-time graph of the Landers Earthquake is shown in Figure 3.6.

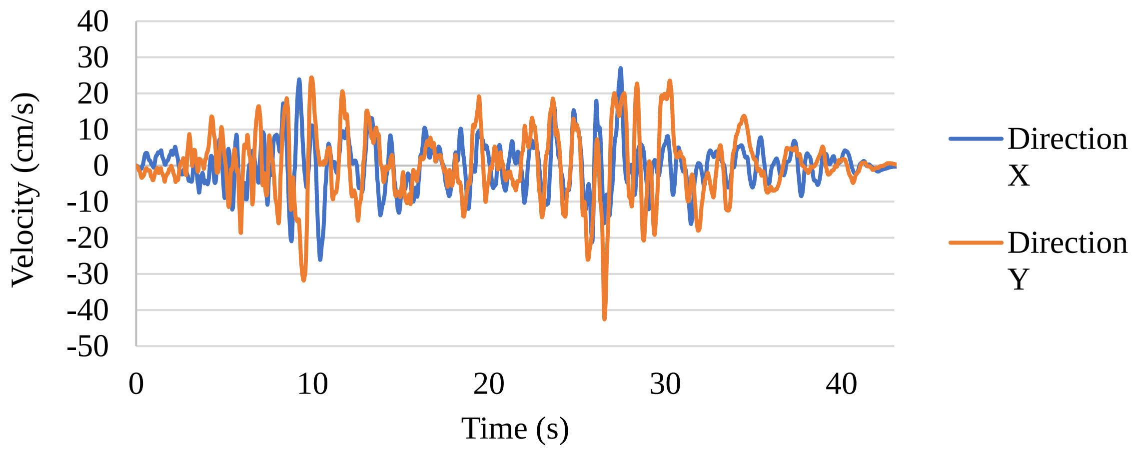

Figure 3.6 : Velocity–time plot of earthquake record RSN 864 (Landers).

The displacement-time graph of the Landers Earthquake was examined for the x direction, and the peak displacement of 7.711 cm was observed at 13.60 s. For the y direction, a displacementof 15.77 cm occurred at 26.90 s. The displacement-time graph of the Landers Earthquake is shown in Figure 3.7.

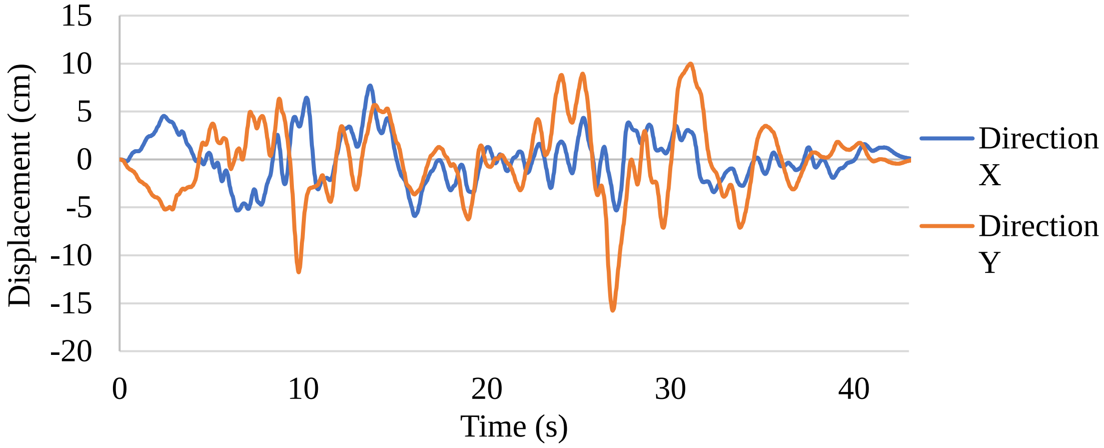

Figure 3.7 : Displacement–time plot of earthquake record RSN 864 (Landers).

3.1.5 Matching of earthquake records to the design spectrum

The selected earthquake records were incorporated into the design analysis following the methods recommended by the Turkish Seismic Code (TSC, 2018). According to the code, acceleration records are used to determine the map-based spectral acceleration coefficients corresponding to the location of the structure, and from these coefficients, the design acceleration parameters are calculated. Based on the obtained values, the horizontal elastic design spectrum is constructed, where the abscissa of the graph represents the periods and the ordinate represents the horizontal elastic design spectral accelerations. A spectrum matching procedure was carried out using the SeismoMatch software to enable the selected earthquake record to better represent the region-specific seismic characteristics.

The design ground motion was chosen to be the DD-2 earthquake. This motion is a rare seismic event with a 475-year return time and a 10% possibility of exceeding it in 50 years. The earthquake data were obtained from a location at 41.010778° latitude and 28.860398° longitude via the AFAD Interactive Web Application of Turkey Earthquake Hazard Maps (URL-7). For soil–structure interaction, the soil type was classified as ZC based on the measured sample values, and the corresponding design spectrum information for the selected region (Bahçelievler, Istanbul) is presented in Table 3.5.

Table 3.5 : Design spectrum parameters selected for the Bahçelievler/İstanbul region.

Parameters	**Values**
Soil Class	ZC
Design Earthquake	DD-2
Peak Ground Acceleration (PGA)	0.432 (g)
Peak Ground Velocity (PGV)	26.448 cm/s
Short-Period Mapped Spectral Acceleration Parameter (S_s)	1.051
Mapped Spectral Acceleration Parameter at 1.0 s Period (S_1)	0.290
Short-Period Site Coefficient (F_s)	1.200
Site Coefficient at 1.0 s Period (F_1)	1.500
Short-Period Design Spectral Acceleration Parameter (S_{DS})	1.261
Design Spectral Acceleration Parameter at 1.0 s Period (S_{D1})	0.435
Corner Period of Horizontal Elastic Design Acceleration Spectrum (T_A)	0.069 s
Corner Period of Horizontal Elastic Design Acceleration Spectrum (T_B)	0.345 s

Figure 3.8 displays the design spectrum computed for the Kocaeli Earthquake, and Figure 3.9 displays the acceleration-time histories. The elastic design graph based on the original earthquake records lies below the spectrum drawn for the ZC soil class and DD-2 design motion (Figure 3.9). The design approach aims to increase the internal forces in the structure, allowing for appropriate calculations under this condition. In order to fit the required spectrum, the original earthquake records were scaled using predetermined ratios. Additionally, the second chapter of TSC 2018 outlines the general procedure for scaling earthquake records using a simple scaling method.

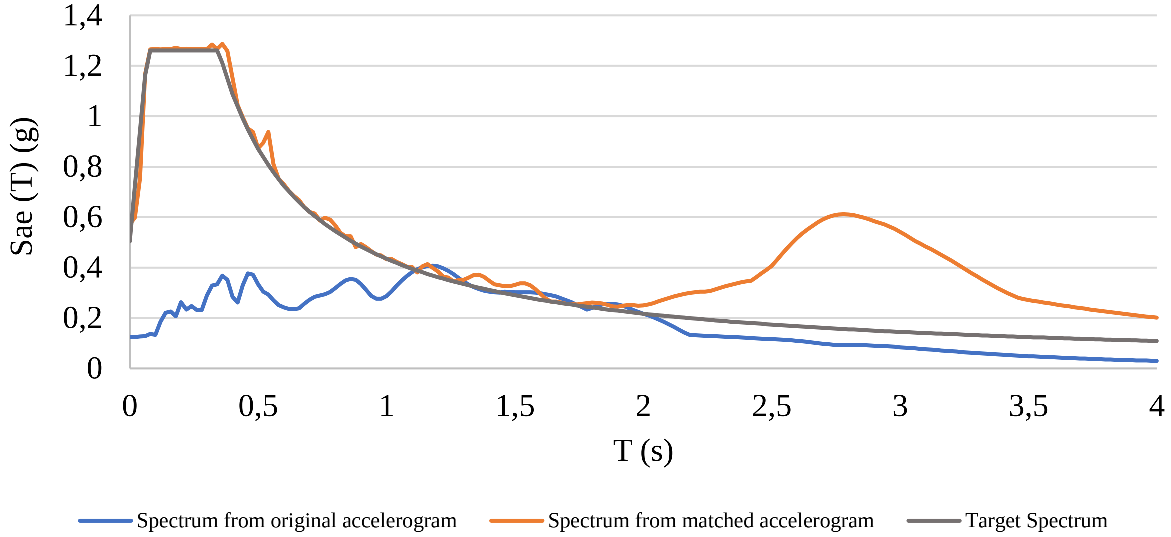

Figure 3.8 : Comparison of the Kocaeli Earthquake spectrum with the design spectrum.

The original and matched acceleration values of the Kocaeli Earthquake are presented in Figure 3.9. The matched values are significantly higher than the original ones.

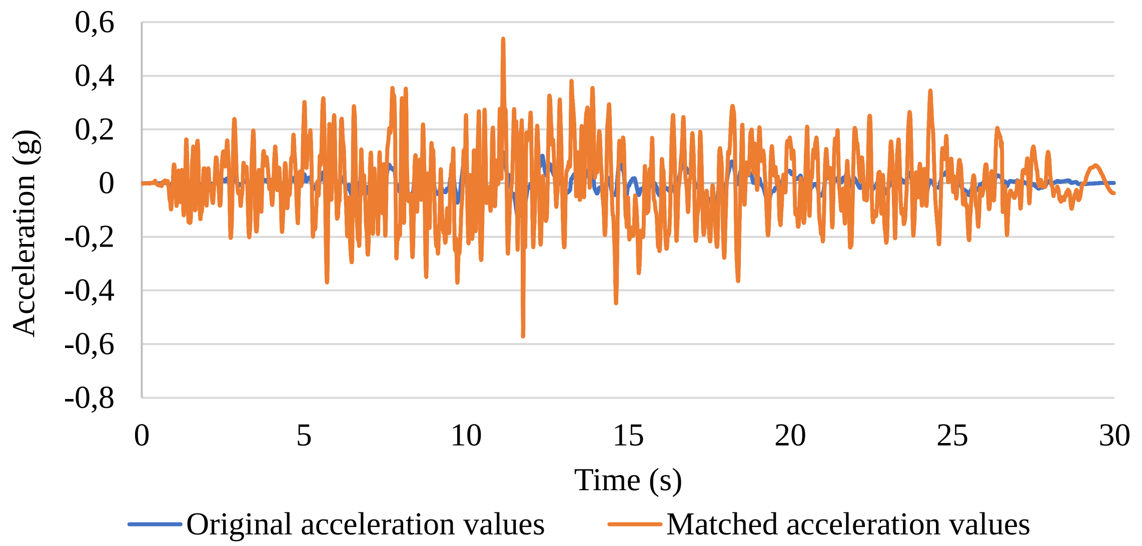

Figure 3.9 : Comparison of the Kocaeli Earthquake acceleration with the design accelerations.

Figure 3.10 displays the design spectrum computed for the Landers Earthquake, and Figure 3.11 displays the matching acceleration-time histories. These numbers offer a thorough depiction of the seismic demand, enabling a thorough comparison between the design parameters utilized in the structural study and the first features of the earthquake.

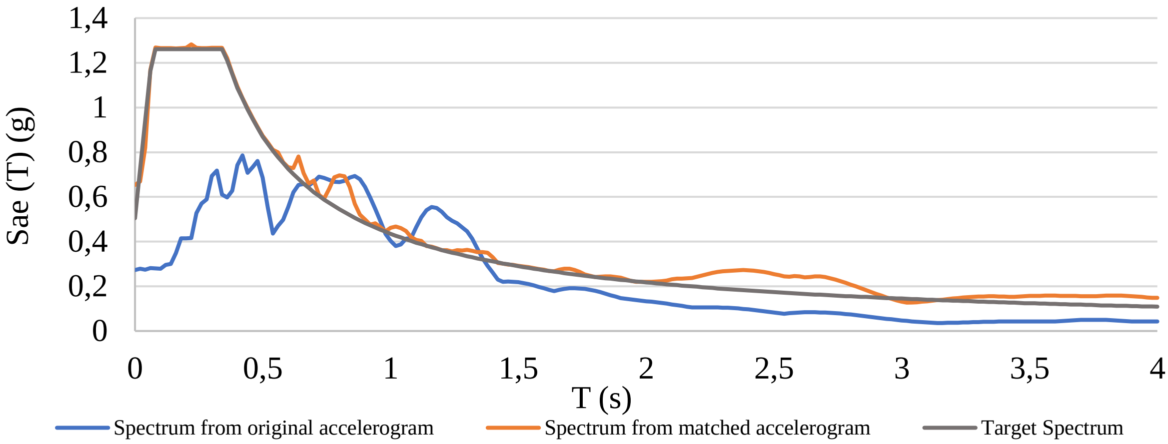

Figure 3.10 : Comparison of the Landers Earthquake spectrum with the design spectrum.

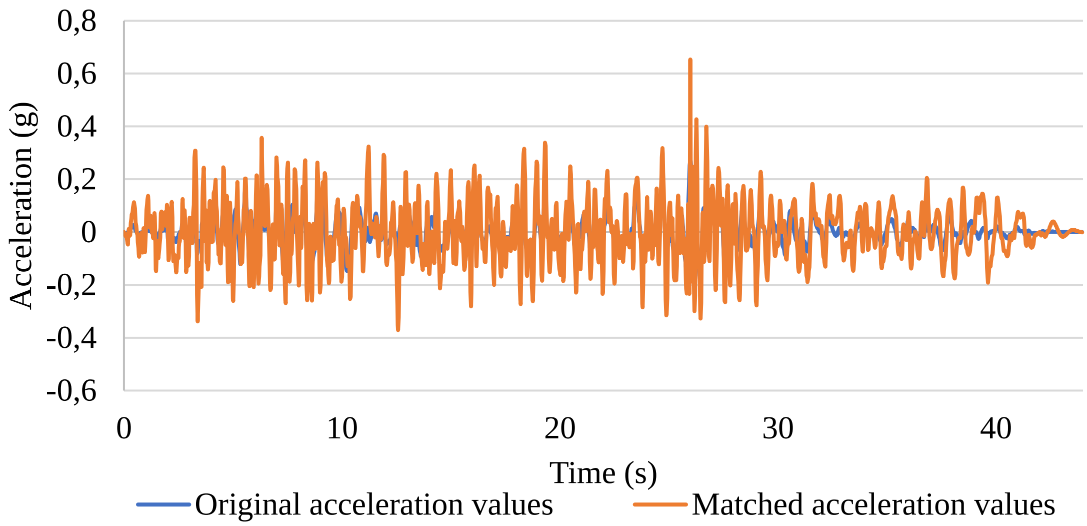

Figure 3.11 : Comparison of the Landers Earthquake acceleration with the design accelerations.

3.1.6 Identification of the seismic isolators

Earthquake-induced ground movements propagate through the ground, reaching the structure and causing significant impacts. Various engineering methods exist to mitigate these effects, one of which is seismic isolators. Seismic isolators are parts placed between the structure and the ground to reduce the forces transferred from the ground to the structure during an earthquake. By lengthening the structure's effective period, these solutions considerably lower the internal forces produced in the superstructure, hence minimizing the amplitude of the earthquake loads. The two types of isolators that are commonly used in this thesis are lead rubber bearing and high damping rubber bearing isolators.

3.1.7 Lead rubber bearing (LRB)

One popular kind of seismic isolator intended to increase the flexibility of structures exposed to seismic forces is the lead rubber bearing (LRB). The system is made up of steel and rubber layers that alternate with a central lead core. The rubber layers generate elastic deformation, while the lead core dissipates seismic energy. Figure 3.12 shows the lead-rubber bearing's layered design, which includes the placement of the steel and elastomer layers.

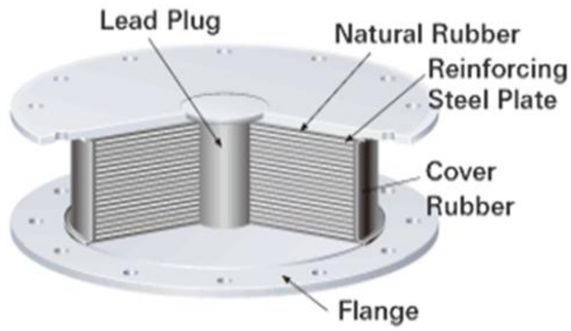

Figure 3.12 : LRB layers (URL-2).

LRBs are widely implemented in buildings and bridges located in high seismic risk areas to enhance structural resilience. The vertical load transfer of the LRB-type lead-rubber seismic isolator is achieved through multiple layers, including the beam body, upper and lower connection steel plates, upper and lower sealing plates, and the laminated rubber with a central lead core (URL-8). This design also eliminates the need for a separate damper, making LRBs particularly suitable for installations where space is limited (URL-2). The LRB isolators used in this thesis were selected from the catalog, taking into account the column dimensions and the loads applied to the columns. The total building weight was found to be 18.600 kN, resulting in a unit load of 1.162,50 kN per isolator. An LRB isolator with a total rubber thickness of 200 mm, corresponding to the Bridgestone catalog code LH085G4, was selected for this study (URL-2). The properties of the isolators, both selected and calculated, are presented in Table 3.6

Table 3.6 : LRB design parameters.

Parameter	**Value**
Outer Diameter of Isolator (mm)	850
Diameter of Elastomer Plate Bonded to Steel (mm)	830
Lead Core Diameter (mm)	120
Shear Yield Stress of Lead (MPa)	8
Rubber Shear Modulus (MPa)	0,385
Total Height of Isolation Unit (mm)	413.1
Total Elastomer Thickness (mm)	200
Elastomer Layer Thickness (mm)	5.7
Lead Core Cross-sectional Area (mm^2)	11.309,7
Surface Area of Single Elastomer Layer Bonded to Steel (mm^2)	529.751,1
Shape Coefficient of Elastomer Isolation Unit	35.6
Modulus of Elasticity of Rubber (MPa)	1.54
Rubber Material Hardness	0.85
Compressive Modulus of Isolation Unit (MPa)	3.327,428
Rubber Volume Modulus	2000
Vertical Stiffness Modulus (MPa)	1.249,169
Vertical Stiffness of Isolation Unit (kN/m)	3.308.742

3.1.8 High damping rubber bearing (HDRB)

A high damping rubber bearing (HDRB) was utilized in this investigation. In contrast to natural rubber bearings, HDRBs are made with rubber compounds that have been carefully designed to have inherent energy dissipation capacity. As a result, HDRBs exhibit stable hysteretic behavior with relatively high equivalent damping ratios, typically ranging between 10% and 20%, without the need for additional damping devices (URL-2). Over a broad range of shear deformations, the restoring force characteristics of HDRBs stay steady and smooth. In this work, the HDRB system was modeled without additional dampers to directly evaluate the effect of inherent damping properties of different types of isolators on the seismic response of the structure.

The layered structure of a high damping rubber (HDRB) is depicted in Figure 3.13, which also shows how the steel and elastomer layers are arranged inside the isolator.

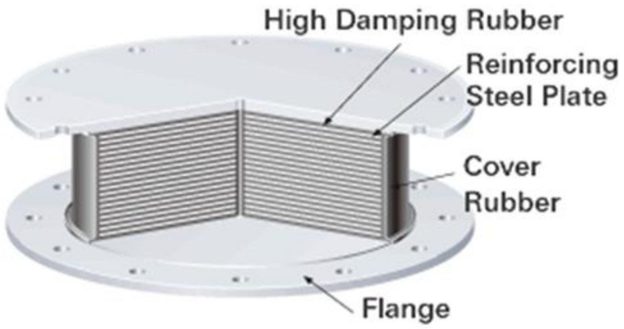

Figure 3.13 : HDRB layers (URL-2).

HDRB with a total rubber thickness of 160 mm, corresponding to the Bridgestone catalog code HM060X3R, was selected for this study (URL-2). The properties of the HDRB isolators selected for this study are summarized in Table 3.7. These parameters include the geometric dimensions, material characteristics, and mechanical properties that are essential for accurately modeling the isolators' behavior under seismic loading. The table provides a comprehensive overview of the isolators' design values, which form the basis for analyses.

Table 3.7 : HDRB design parameters.

Parameter	**Value**
Outer Diameter of Isolator (mm)	600
Inner Diameter (mm)	15
Rubber Shear Modulus (MPa)	0.3
Total Height of Isolation Unit (mm)	294.1
Total Elastomer Thickness (mm)	160
Elastomer Layer Thickness (mm)	5
Shape Coefficient of Elastomer Isolation Unit	29.3
Rubber Material Hardness	1
Rubber Volume Modulus	2.000
Vertical Stiffness Modulus (MPa)	2.55
Vertical Stiffness of Isolation Unit (kN/m)	1.740.000

4. ANALYSIS RESULTS UNDER SEISMIC LOADING

A fixed-base model was implemented in this study, and both LRB and HDRB systems were used to describe seismic isolation. A time-history investigation of two different earthquake ground motions was conducted. The Kocaeli (1999) and Landers (1992) earthquakes were chosen. This section discusses the findings of all analyses that were conducted in the time domain. Nonlinear link elements in SAP2000 were used to represent the isolators, where axial stiffness, lateral stiffness, and hysteretic behavior were explicitly defined. LRBs were modeled using a bilinear force–displacement relationship to capture lead yielding and post-yield stiffness, whereas HDRBs were modeled with nonlinear elastic behavior and higher equivalent damping ratios.

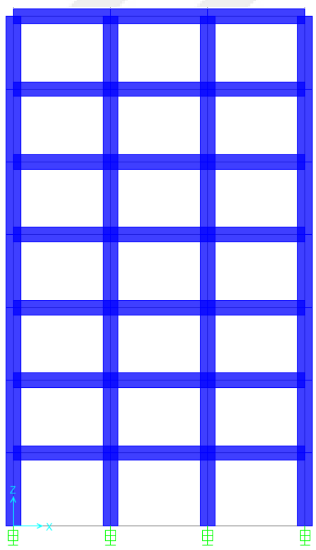

Figure 4.1 : Structural model with LRB.

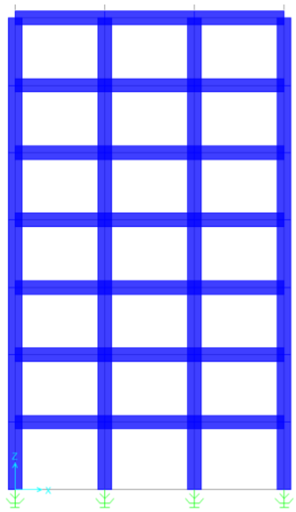

Figure 4.2 : Structural model with HDRB.

4.1 Time-History Analysis of the Kocaeli Earthquake

The results of a time history study conducted under the Kocaeli Earthquake are shown in this section. As Table 4.1 illustrates, the investigation shows that isolators significantly affect the building's dynamic behavior.

Table 4.1 : Comparison of structural period, base shear, and overturning moment of the models under the Kocaeli Earthquake.

Model	**Structural Period**	**Overturning Moment in X Direction (kNm)**	**Overturning Moment in Y Direction (kNm)**	**Base Shear in X Direction (kN)**	**Base Shear in Y Direction (kN)**
Fixed	T1=0.60 s	20590	30210	2290	2007
LRB	T1=1.77 s	15110	22930	1750	1313
HDRB	T1=2.38 s	14130	15460	1323	1139

The fixed-base structure's fundamental period is 0.60 seconds, indicating relatively stiff structural behavior. When LRBs are implemented, the period increases to 1.77 seconds, corresponding to an increase of approximately 195% compared to the fixed-base condition. With the use of HDRB, the period is further extended to 2.38 seconds, representing an increase of about 297% relative to the fixed-base structure. By extending the building's vibration period, seismic isolators lower the quantity of seismic energy that is transferred to the structure.

The fixed-base structure exhibits overturning moments of 20.590 kNm in the X-direction and 30.210 kNm in the Y-direction. With the implementation of LRB, these values decrease to 15.110 kNm and 22.930 kNm, corresponding to reductions of approximately 26.6% and 24.1% in the X- and Y-directions, respectively. Further reductions are observed with HDRB, resulting in overturning moments of 14.130 kNm in the X-direction and 15.460 kNm in the Y-direction. Compared to the fixed-base structure, this represents reductions of approximately 31.4% in the X-direction and 48.8% in the Y-direction. The use of isolators significantly reduces the moments, especially in the upper stories. Base shear forces show a similar trend. In the fixed-base structure, the base shear forces are 2.290 kN and 2.007 kN in the X and Y directions, respectively. With the implementation of LRB, these values decrease to 1.750 kN in the X-direction and 1.313 kN in the Y-direction, corresponding to reductions of approximately 23.6% and 34.6%, respectively. Further reductions are achieved with the use of HDRB, resulting in base shear forces of 1.323 kN in the X-direction and 1.139 kN in the Y-direction. Compared to the fixed-base structure, this represents reductions of approximately 42.2% in the X-direction and 43.2% in the Y-direction. Isolators distribute the seismic load at the base, reducing the forces transmitted to the upper stories. Energy dissipation in LRB occurs through both the elastomer layers and the lead core at the center, with the lead core absorbing part of the seismic energy through plastic deformation. In HDRB, energy dissipation is provided by the high-damping elastomer material, offering a more uniform and higher damping capacity compared to LRB. In conclusion, both LRB and HDRB reduce overturning moments and base shear forces, increase the fundamental period, and improve the seismic performance of the building compared to a fixed-base structure.

Figure 4.3 presents the distributions of relative story displacements for the fixed-base, LRB, and HDRB structural systems under the Kocaeli earthquake. Figure 4.4 provides the corresponding displacement–time histories for the top story. In the fixed-base system, the relative story displacements increase steadily with building height and reach their maximum values at the upper stories. This behavior indicates that, in rigidly supported structures, seismic effects are directly transmitted to the superstructure, resulting in significantly increased story deformation demands at higher levels. In contrast, the base-isolated systems exhibit considerably lower relative story displacements compared to the fixed-base structure. In particular, the models employing LRB and HDRB isolators show higher relative displacements at the lower stories, followed by a decreasing trend toward the upper stories. This response demonstrates that seismic isolation effectively dissipates a substantial portion of the seismic energy at the foundation level, thereby limiting deformation demands in the superstructure. A comparison between the LRB and HDRB systems reveals that the HDRB model produces lower relative story displacement values than the LRB model across all story levels. This outcome can be attributed to the higher effective damping capacity and more stable hysteretic behavior of the HDRB system, which enables a more efficient reduction of deformation demands in the superstructure. In conclusion, under strong ground motions such as the Kocaeli earthquake, base-isolated systems significantly reduce relative story displacements in the superstructure and substantially improve structural performance when compared to the fixed-base configuration.

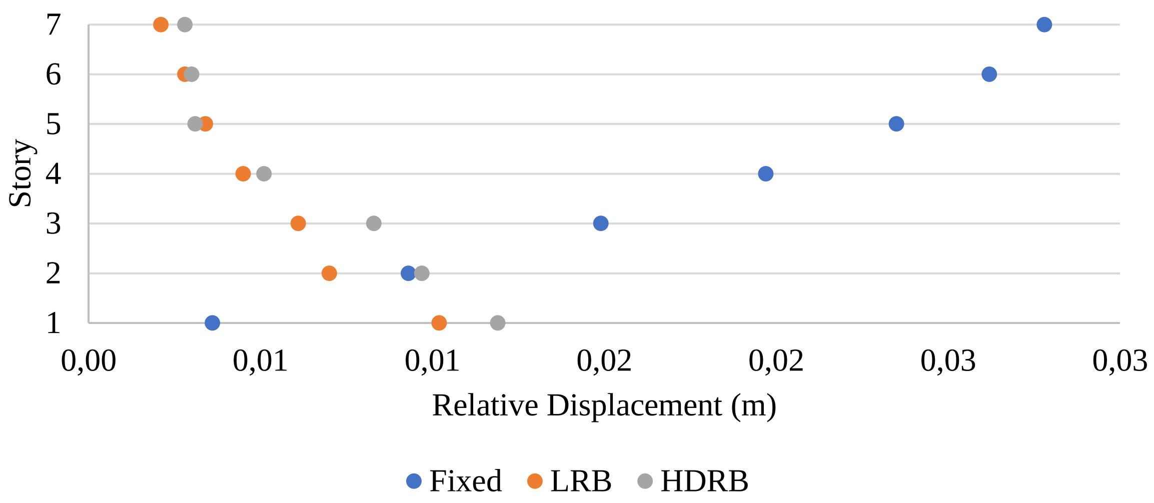

Figure 4.3 : Distribution of maximum story displacements under the Kocaeli Earthquake.

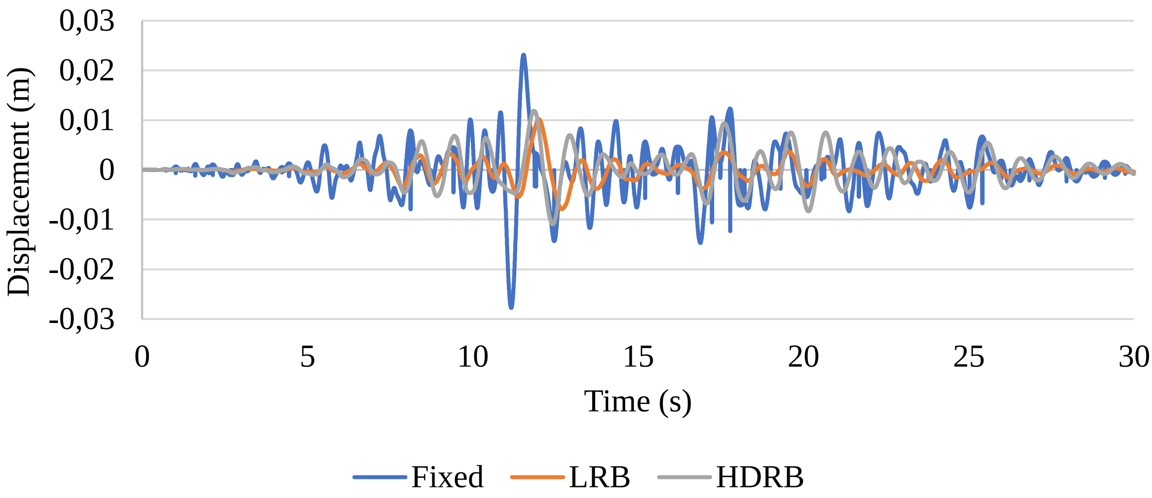

Figure 4.4 : Top-story displacement–time plots under the Kocaeli Earthquake.

In Figure 4.5, the story velocity distributions for fixed-base, LRB, and HDRB systems under the Kocaeli earthquake are presented, while Figure 4.6 shows the corresponding velocity–time histories. It is observed that, in the fixed-base system, story velocities increase regularly with building height, reaching maximum values at the upper stories. In contrast, in the base-isolated systems, story velocities are significantly reduced and exhibit a more uniform distribution across the stories. Compared to the fixed-base structure, both the LRB and HDRB systems significantly reduce velocity demands; however, the HDRB model generally exhibits lower velocity values overall.

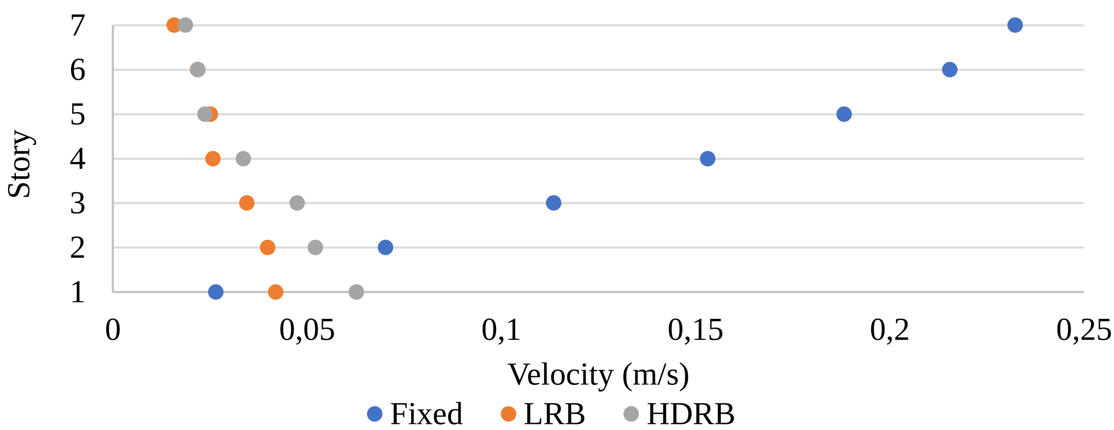

Figure 4.5 : Distribution of maximum velocities under the Kocaeli Earthquake.

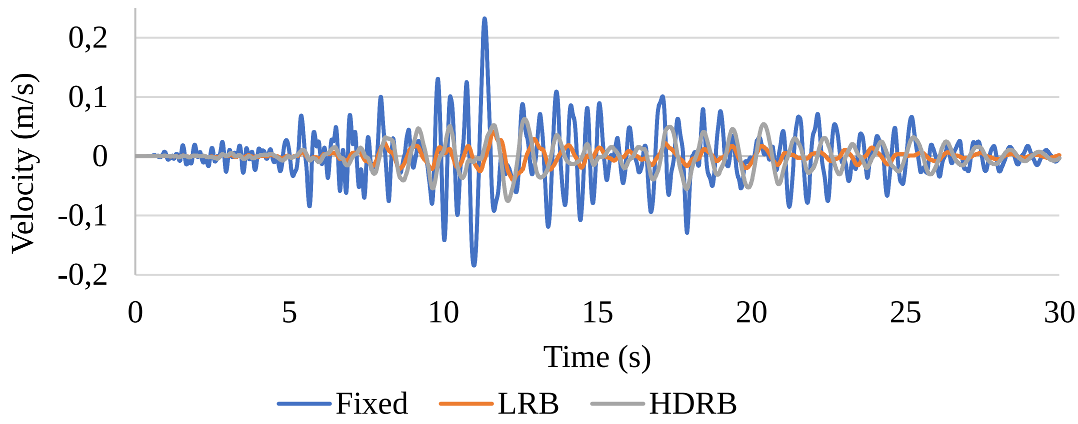

Figure 4.6 : Top-story velocity–time plots under the Kocaeli Earthquake.

Figure 4.7 presents the story acceleration distributions for the fixed-base, LRB, and HDRB systems under the Kocaeli earthquake, while Figure 4.8 shows the corresponding acceleration–time histories for the top story. The fixed-base system exhibits a clear increase in story accelerations with building height, with the upper stories experiencing the highest demands. In contrast, the LRB and HDRB base-isolated systems significantly reduce acceleration levels throughout the structure, providing a more uniform response across the stories. Between the two isolation systems, the HDRB demonstrates slightly better performance, yielding lower accelerations overall and effectively dissipating seismic energy. When compared to the fixed-base system, these results demonstrate that seismic isolation effectively reduces seismic demands and enhances the overall structural response.

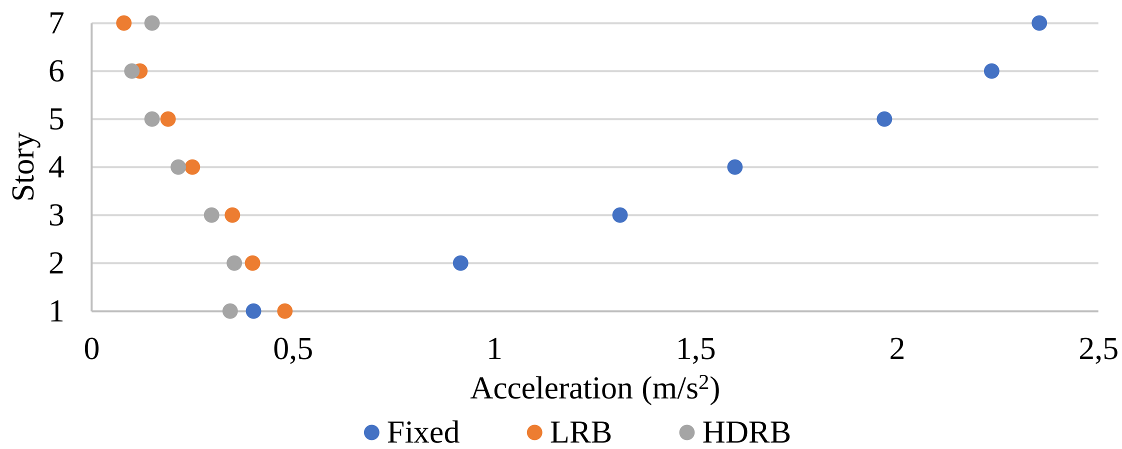

Figure 4.7 : Distribution of maximum story accelerations under the Kocaeli Earthquake.

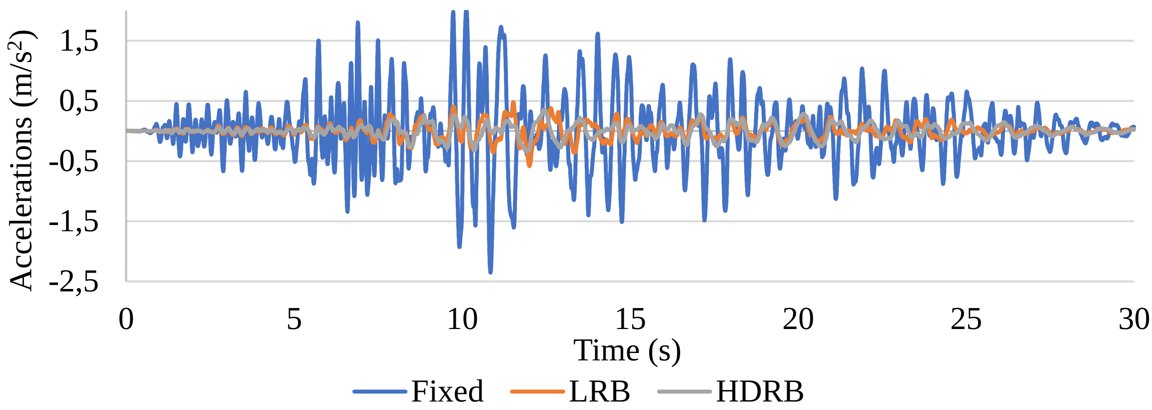

Figure 4.8 : Top-story acceleration–time plots of under the Kocaeli Earthquake.

4.2 Time-History Analysis of the Landers Earthquake

Table 4.2 displays the seismic response outcomes of the fixed-base, LRB-isolated, and HDRB-isolated structural models that were exposed to the Landers earthquake. Base shear forces and overturning moment demands in both principal horizontal directions are compared.

Table 4.2 : Comparison of structural period, base shear, and overturning moment of the models under the Landers Earthquake

Model	**Structural Period**	**Overturning Moment in X Direction (kNm)**	**Overturning Moment in Y Direction (kNm)**	**Base Shear in X Direction (kN)**	**Base Shear in Y Direction (kN)**
Fixed	T1=0.60 s	70530	71360	4997	5537
LRB	T1=1.77 s	26430	24940	2008	2109
HDRB	T1=2.38 s	19310	10390	882	1473

As observed in Table 4.2, the fixed-base structure exhibits the highest base shear and overturning moment demands in both horizontal directions. This behavior is primarily associated with the relatively short fundamental period of the fixed-base system, which leads to increased seismic force demands under the long-period characteristics of the Landers earthquake. The implementation of seismic isolation significantly reduces both base shear and overturning moments. The LRB-isolated structure demonstrates a considerable decrease in seismic demands compared to the fixed-base model due to period elongation and energy dissipation provided by the lead core. Furthermore, the HDRB isolated structure yields the lowest base shear and overturning moment values among all configurations. This response can be attributed to the higher inherent damping capacity of HDRB systems, which is particularly effective in mitigating long-period ground motion effects. Additionally, the differences observed between the X and Y direction responses indicate the influence of directional ground motion characteristics, which become more pronounced in base-isolated systems due to their increased flexibility.

In Figure 4.9, the story relative displacement distributions for fixed-base, LRB, and HDRB systems are presented, while Figure 4.10 shows the corresponding displacement–time histories. The fixed-base structure exhibits significantly higher relative displacement demands at all story levels, indicating increased deformation sensitivity to long-period ground motion. This behavior highlights the vulnerability of rigidly supported structures when subjected to earthquakes characterized by long duration and dominant low-frequency content. Both base-isolated configurations demonstrate a marked reduction in relative displacements compared to the fixed-base system. The LRB-isolated structure shows consistently low and well-distributed relative displacements, suggesting that the combined effect of period elongation and hysteretic damping effectively limits deformation demands under long-period excitation. The HDRB-isolated structure exhibits relatively higher displacement demands than the LRB system, particularly at lower story levels. This behavior is primarily attributed to the higher flexibility of HDRB bearings, which allows greater isolation-level deformation under long-period seismic inputs. The HDRB system's substantially lower total displacement response as compared to the fixed-base structure confirms the efficacy of high-damping rubber bearings in reducing the seismic effects of the Landers earthquake.

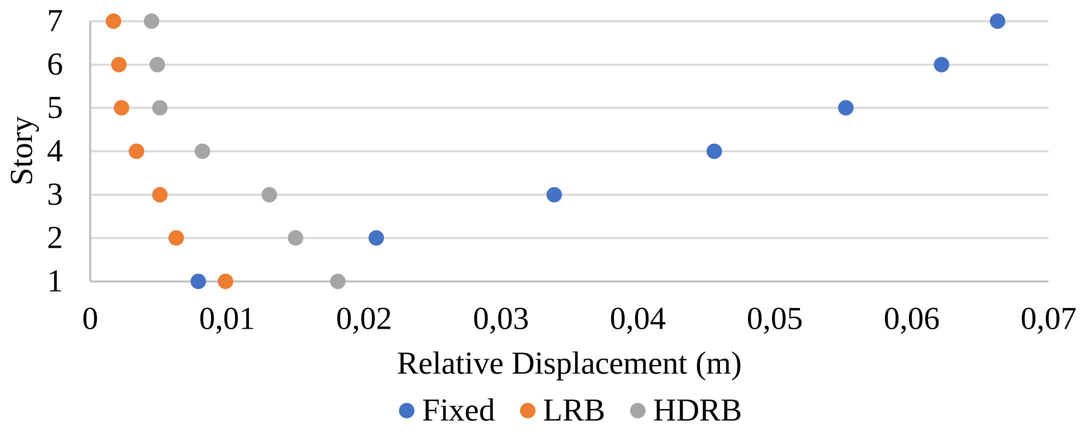

Figure 4.9 : Distribution of maximum story relative displacement under the Landers Earthquake.

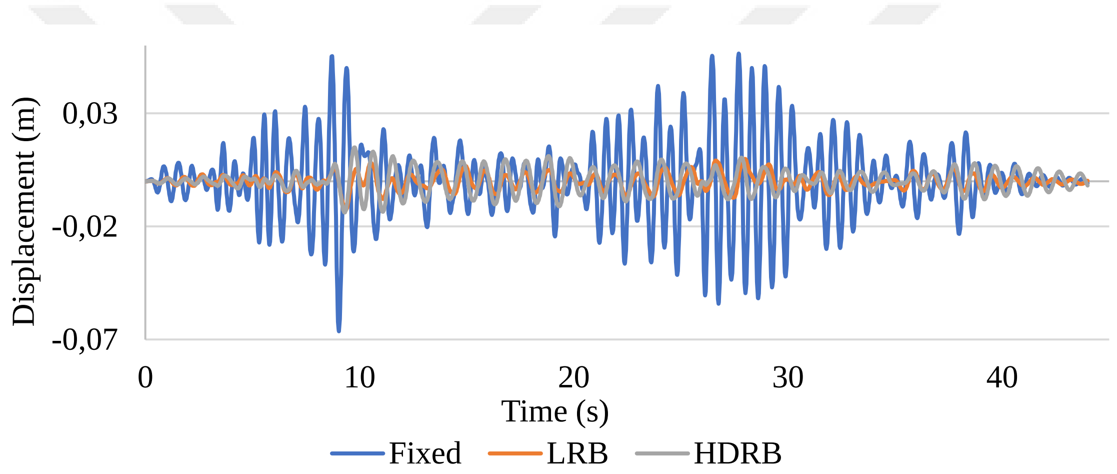

Figure 4.10 : Top-story displacement–time plots under the Landers Earthquake.

In Figure 4.11, the story velocity distributions for fixed-base, LRB, and HDRB systems are presented, while Figure 4.12 shows the corresponding velocity–time histories. The fixed-base system exhibits increasing story velocities with height, reaching the highest values at the top stories. In contrast, both LRB and HDRB base-isolated systems considerably reduce velocities throughout the structure, providing a more uniform response across the stories. Between the two isolation systems, HDRB generally produces slightly higher velocities at the lower stories but maintains effective mitigation overall. seismic isolation

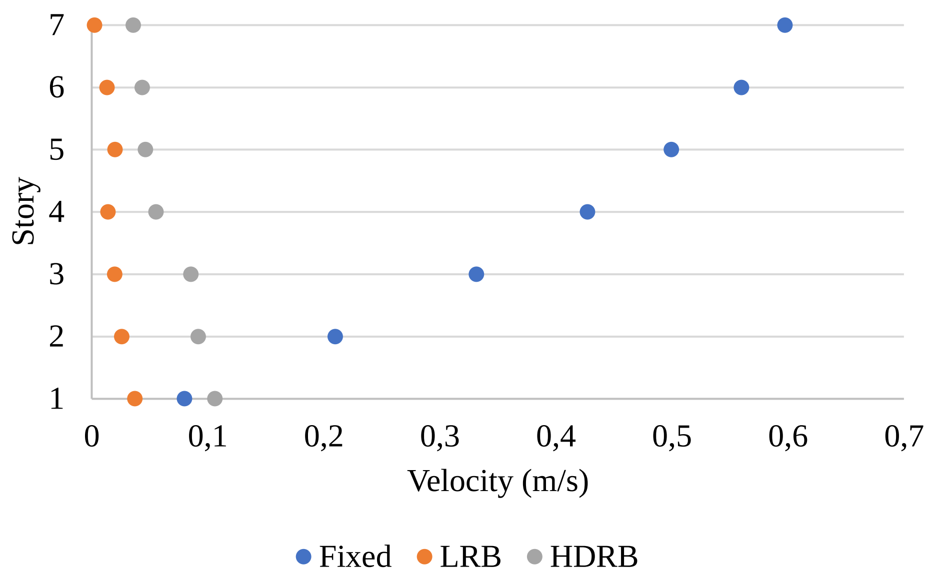

Figure 4.11 : Distribution of maximum velocities under the Landers Earthquake.

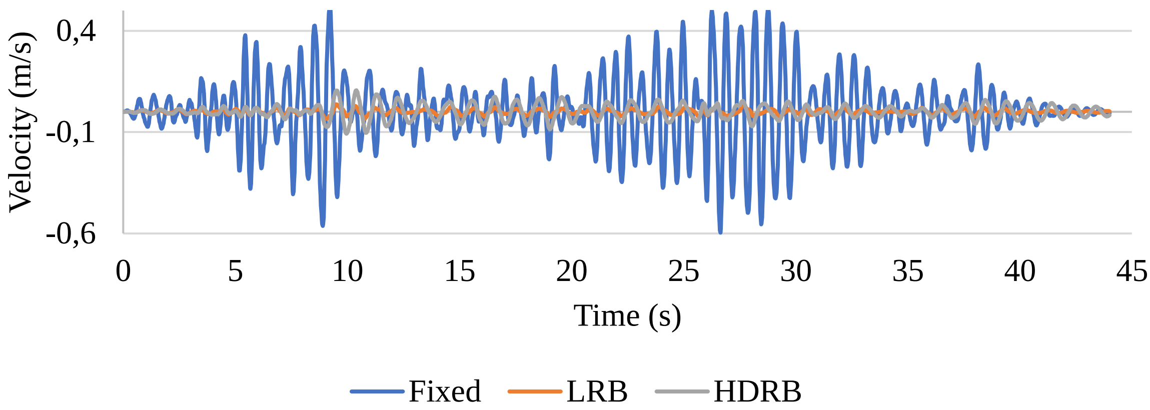

Figure 4.12 : Top-story velocity–time plots under the Landers Earthquake.

Figure 4.13 presents the maximum story acceleration distributions for the fixed-base, LRB, and HDRB systems under the Landers earthquake, while Figure 4.14 shows the corresponding acceleration–time histories for the top story. The fixed-base system shows a clear increase in story accelerations with building height, with the upper stories experiencing the largest demands. In contrast, the LRB and HDRB base-isolated systems significantly reduce accelerations throughout the structure, leading to a more uniform and controlled response. Among the isolation systems, HDRB demonstrates slightly better performance in reducing overall accelerations, particularly in the upper stories. seismic isolation

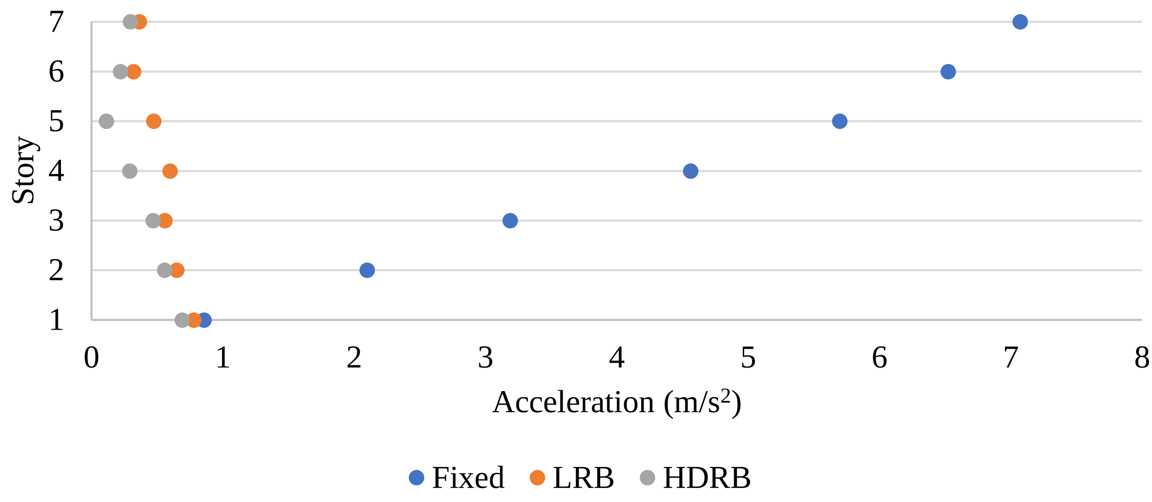

Figure 4.13 : Distribution of maximum story accelerations under the Landers Earthquake.

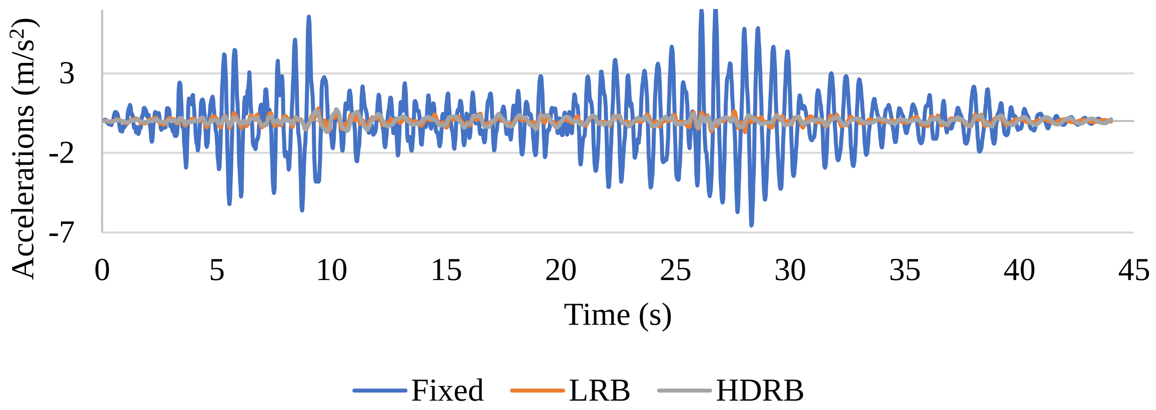

Figure 4.14 : Top-story acceleration–time plots under the Landers Earthquake.

4.3 Time-History Analysis of the Kocaeli Earthquake with Reduced Material Strentgh

In this section, the structural geometry and system configuration used in the previous analyses are maintained, while the material properties are modified by adopting C15 concrete and BC1 reinforcing steel. This approach is adopted to better represent the characteristics of the existing older building stock. This configuration is referred to as the reduced material strength model, whereas the model constructed using C30 concrete and B420C reinforcing steel is defined as the reference model. Time-history analyses are carried out on the same structural model using identical earthquake records in order to ensure a consistent basis for comparison. Fixed-base, LRB-isolated, and HDRB-isolated systems are analyzed separately, and the results obtained from the reduced material strength model are comparatively evaluated with those of the reference model. Table 4.3 presents the comparison of structural period, base shear, and overturning moment of the reduced material strength models under the Kocaeli Earthquake.

Table 4.3 : Comparison of structural period, base shear, and overturning moment models under the Kocaeli Earthquake with reduced material strength.

Model	Structural Period	Overturning Moment in X Direction (kNm)	Overturning Moment in Y Direction (kNm)	Base Shear in X Direction (kN)	Base Shear in Y Direction (kN)
Fixed	T1=0.66 s	25550	43190	3385	1507
LRB	T1=1.80 s	15270	20920	1730	1375
HDRB	T1=2.41 s	19340	30180	2186	1380

The fundamental period of the fixed-base structure is 0.66 seconds, indicating that the global dynamic response is largely governed by geometric properties and mass distribution rather than material strength. When LRB isolators are introduced, the fundamental period increases to 1.80 seconds, corresponding to an increase of approximately 173% compared to the fixed-base configuration. With the implementation of HDRB, the period is further extended to 2.41 seconds, representing an increase of about 265% relative to the fixed-base structure. These findings show that, even for low-strength material qualities, seismic isolation successfully extends the structure's vibration period and moves the dynamic response away from the ground motion's dominating frequency range.

For the fixed-base structure, the overturning moments are 25.550 kNm in the X-direction and 43.190 kNm in the Y-direction. With the use of LRB isolators, these values are reduced to 15.270 kNm and 20.920 kNm, corresponding to reductions of approximately 40.2% and 51.6% in the X- and Y-directions, respectively. When HDRB isolators are implemented, the overturning moments become 19.340 kNm in the X-direction and 30.180 kNm in the Y-direction. Compared to the fixed-base structure, these results indicate reductions of approximately 24.3% in the X-direction and 30.1% in the Y-direction. Although the HDRB system provides significant reductions relative to the fixed-base condition, the LRB system yields lower overturning moments for this material scenario under the Kocaeli earthquake. A similar trend is observed for the base shear forces. In the fixed-base structure, the base shear values are 3.385 kN in the X-direction and 1.507 kN in the Y-direction. With the implementation of LRB, these values decrease to 1.730 kN and 1.375 kN, corresponding to reductions of approximately 48.9% and 8.8%, respectively. For the HDRB-isolated structure, the base shear forces are 2.186 kN in the X-direction and 1,380 kN in the Y-direction, indicating reductions of approximately 35.5% and 8.4% compared to the fixed-base case. These findings show that both isolation systems reduce base shear demands, while the LRB system provides the most effective force reduction for the reduced material strength models under the Kocaeli earthquake. The interplay between the isolation system and the softened superstructure is responsible for the observed behavior. In the reduced material strength models scenario, stiffness degradation in the superstructure limits the efficiency of highly flexible isolation systems, causing the HDRB model to exhibit higher force demands than the LRB model despite its longer fundamental period. Nevertheless, both isolation systems significantly reduce seismic demands compared to the fixed-base structure. Overall, the results confirm that seismic isolation remains effective for low-strength material properties, although the relative performance of LRB and HDRB depends on the compatibility between isolator flexibility and the frequency content of the ground motion.

Figure 4.15 presents the distributions of relative story displacements for the fixed-base, LRB, and HDRB structural systems under the Kocaeli earthquake with reduced material strength. Figure 4.16 provides the corresponding displacement–time histories for the top story with reduced material strength. For the Kocaeli earthquake record, the reduction in material strength results in increased relative story displacements in the fixed-base structure due to the decrease in global stiffness. In contrast, both LRB- and HDRB-isolated models exhibit significantly lower and more uniform interstory displacement demands along the building height. The limited sensitivity of the base-isolated structures to the reduction in material strength indicates that the seismic response is predominantly governed by the isolator characteristics rather than the superstructure stiffness. Although slightly higher relative displacements are observed in the HDRB system compared to the LRB system, the overall drift demands remain substantially lower than those of the fixed-base configuration.

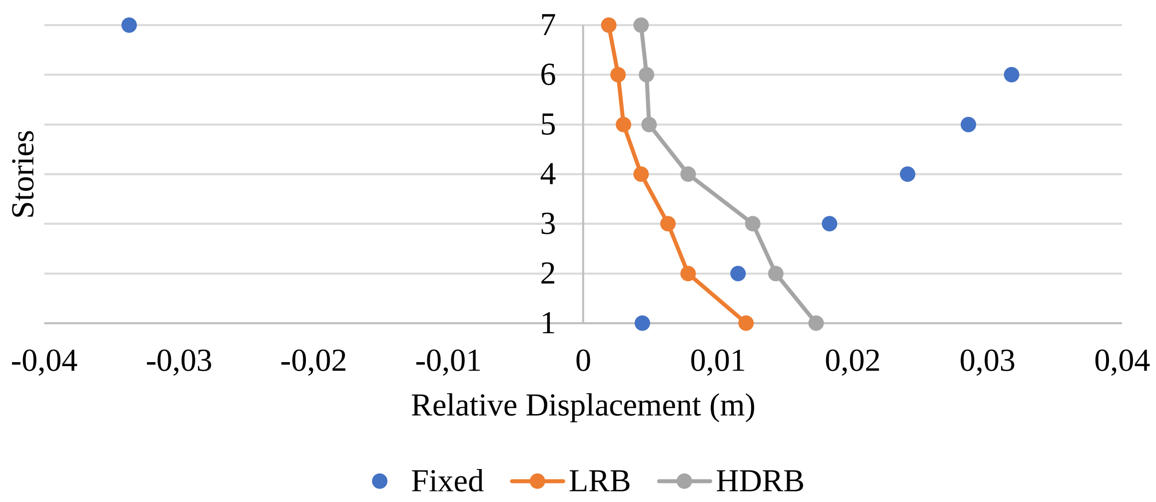

Figure 4.15 : Distribution of maximum story displacements under the Kocaeli Earthquake with reduced material strength.

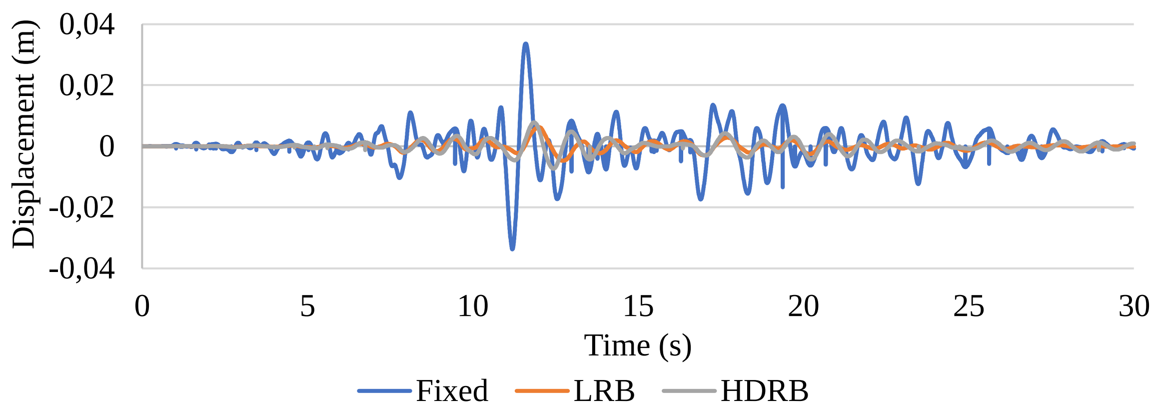

Figure 4.16 : Top-story displacement–time plots under the Kocaeli Earthquake with reduced material strength.

In Figure 4.17, the story velocity distributions for fixed-base, LRB, and HDRB systems with reduced material strength under the Kocaeli earthquake are presented, while Figure 4.18 shows the corresponding velocity–time histories. For the Kocaeli Earthquake, the fixed-base model with reduced material strength exhibits noticeably higher relative story velocities compared to the reference model, particularly in the upper stories, due to decreased structural rigidity. In contrast, LRB- and HDRB-isolated models maintain low and well-distributed velocities along the building height, with the HDRB system showing slightly more uniform distribution. These results indicate that even under reduced material strength, seismic isolation effectively controls velocity demands, while fixed-base systems experience a direct increase in relative velocities.

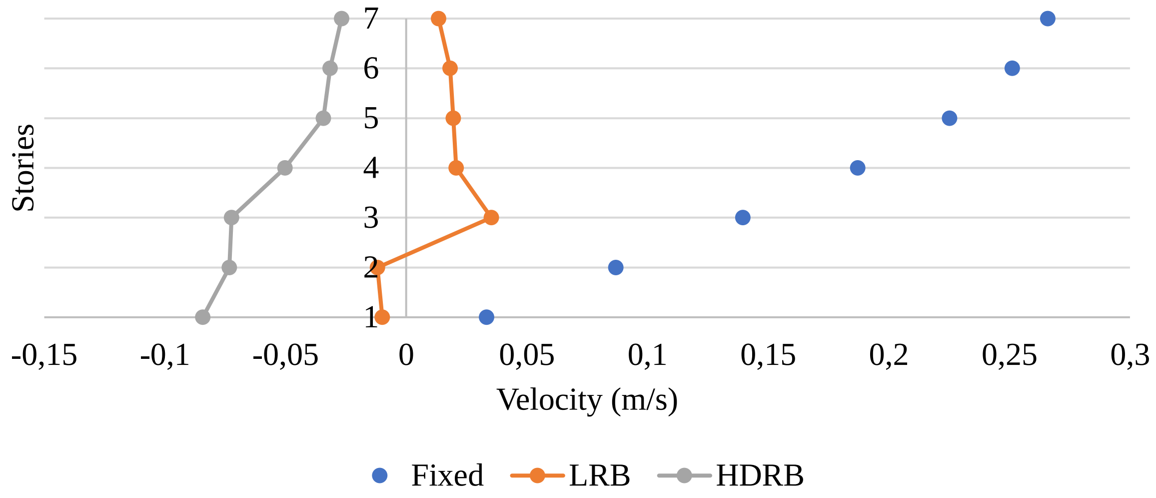

Figure 4.17 : Distribution of maximum velocities under the Kocaeli Earthquake with reduced material strength.

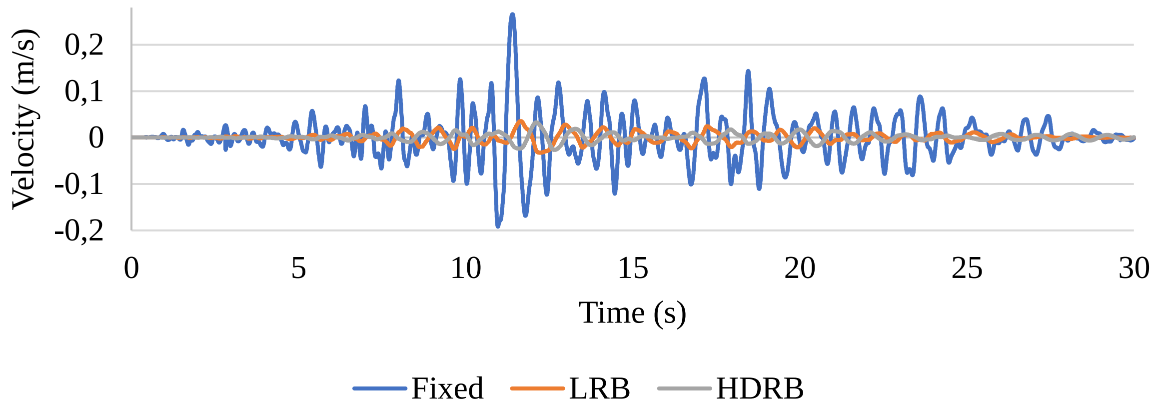

Figure 4.18 : Top-story velocity–time plots under the Kocaeli Earthquake with reduced material strength .

Figure 4.19 presents the story acceleration distributions for the fixed-base, LRB, and HDRB systems under the Kocaeli earthquake with reduced material strength, while Figure 4.20 shows the corresponding acceleration–time histories for the top story. For the Kocaeli Earthquake record, relative story acceleration results indicate that the fixed-base configuration experiences a clear amplification of acceleration demands along the building height, which becomes more pronounced under reduced material strength conditions. Peak acceleration values increase toward the upper stories, reflecting the stronger participation of higher vibration modes in the fixed-base response. In contrast, both LRB- and HDRB-isolated models significantly reduce acceleration transmission to the superstructure. The acceleration profiles of the isolated systems remain low and relatively uniform over the height, demonstrating the filtering effect of the isolation layer. Although minor variations are observed in the reduced material strength case, particularly in the lower stories, the overall acceleration demands in the isolated configurations remain substantially lower than those of the fixed-base system. While fixed-base systems are more susceptible to variations in material qualities in terms of acceleration response, these results demonstrate that seismic isolation is quite successful in regulating floor acceleration demands, even when material strength is decreased.

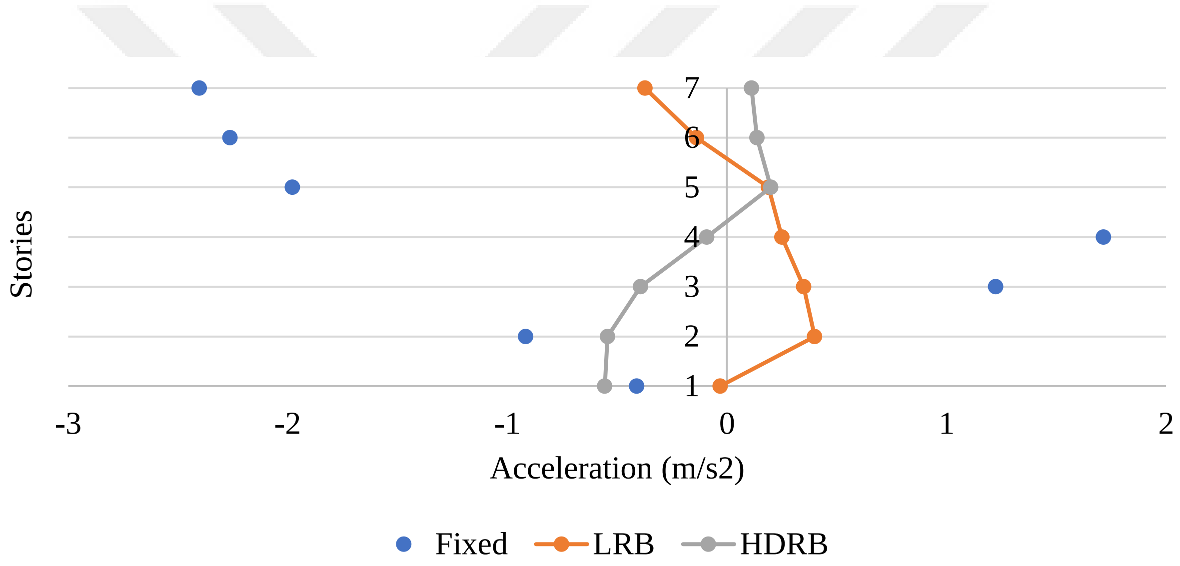

Figure 4.19 : Distribution of maximum story accelerations under the Kocaeli Earthquake with reduced material strength.

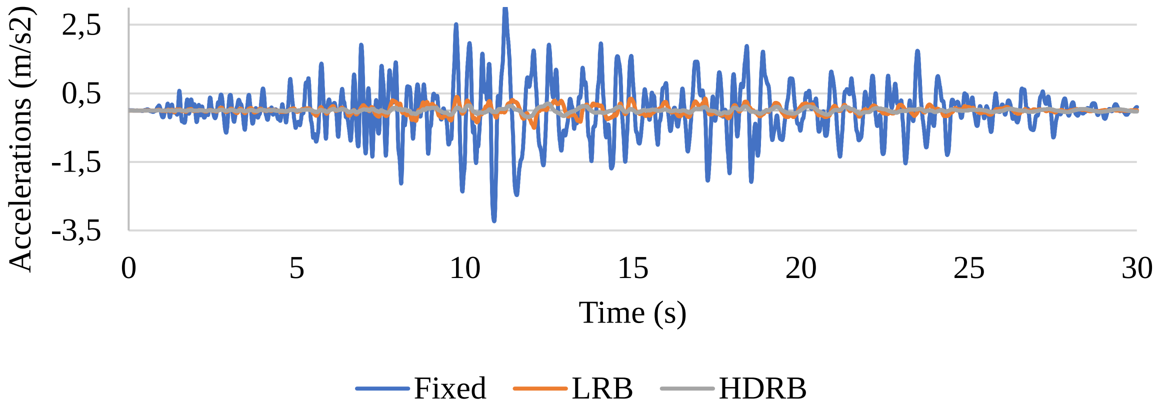

Figure 4.20 : Top-story acceleration–time plots under the Kocaeli Earthquake with reduced material strength.

4.4 Time-History Analysis of the Landers Earthquake with Reduced Material Strength

In this section, time-history analyses of the Landers earthquake are performed on the structural model with reduced material strength models. The analysis results are summarized in Table 4.4.

Table 4.4 : Comparison of structural period, base shear, and overturning moment under the Landers Earthquake with reduced material strength models.

Model	**Structural Period**	**Overturning Moment in X Direction (kNm)**	**Overturning Moment in Y Direction (kNm)**	**Base Shear in X Direction (kN)**	**Base Shear in Y Direction (kN)**
Fixed	T1=0.66 s	94730	79010	5780	7581
LRB	T1=1.80 s	24460	22600	1951	2081
HDRB	T1=2.41 s	54080	47810	3826	5110

As presented in Table 4.4, the fixed-base structure exhibits the highest base shear and overturning moment demands in both horizontal directions. This behavior is mainly associated with the short fundamental period of the fixed-base system (T_1 = 0.66 s), which results in increased seismic demands under the long-period–dominant characteristics of the Landers earthquake. In addition, the reduced material strength in the models configuration contributes to stiffness degradation in the superstructure, further amplifying force demands in the fixed-base case. The introduction of seismic isolation leads to a significant reduction in both base shear forces and overturning moments. Among the isolated configurations, the LRB system provides the most effective performance, yielding the lowest seismic demands. The overturning moments are reduced to 24.460 kNm and 22.600 kNm, while the base shear forces decrease to 1.951 kN and 2.081 kN in the X and Y directions, respectively. This improvement can be attributed to the combined effect of period elongation and stable energy dissipation through the lead core, which is particularly effective for the long-period content of the Landers ground motion.

When compared to the fixed-base system, the HDRB-isolated structure likewise exhibits a discernible decrease in seismic demands; however, its overturning moments (54.080 kNm and 47.810 kNm) and base shear forces (3.826 kN and 5.110 kN) remain higher than those observed for the LRB configuration. Although the HDRB system provides a longer fundamental period (T_1 = 2.41 s) and higher inherent damping, the increased flexibility of the isolation layer, combined with the softened superstructure in the reduced material strength models scenario, leads to higher force demands relative to the LRB system under the Landers earthquake.

The differences observed between the responses in the X and Y directions highlight the influence of directional characteristics of the ground motion, which become more pronounced in base-isolated systems due to their increased flexibility. Overall, the results confirm that seismic isolation remains effective for structures with low-strength material properties. However, the relative performance of isolation systems strongly depends on the interaction between isolator flexibility, superstructure stiffness degradation, and the frequency content of the earthquake record. Under these conditions, the LRB system exhibits the most favorable seismic performance for the reduced material strength models subjected to the Landers earthquake.

In Figure 4.21, the story relative displacement distributions for fixed-base, LRB, and HDRB systems with reduced material strength are presented, while Figure 4.22 shows the corresponding displacement–time histories. For the Landers earthquake record , the fixed-base structure exhibits a significant increase in relative story displacements along the building height in the model with reduced material strength due to the decrease in global stiffness. The long-period characteristics of the Landers ground motion amplify displacement demands in the fixed-base configuration. In contrast, both LRB- and HDRB-isolated models demonstrate substantially lower and more uniform interstory displacement profiles. In the isolated configurations with reduced material strength, relative displacement demands are largely concentrated in the lower stories, while the upper structure responds in a nearly rigid-body manner. This behavior suggests that the isolater behavior, not the superstructure's characteristics, primarily controls the seismic reaction.

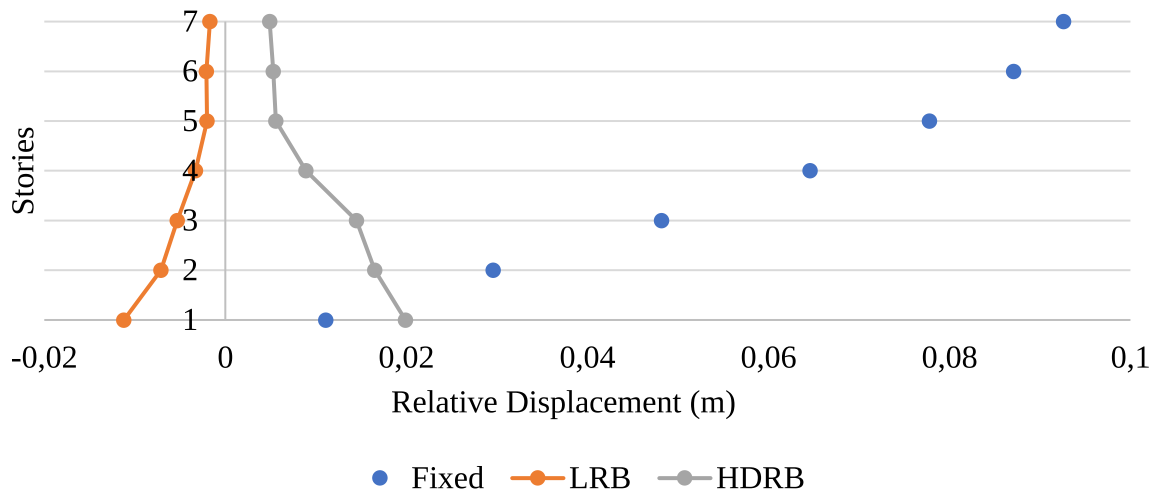

Figure 4.21 : Distribution of maximum story displacements under the Landers Earthquake with reduced material strength.

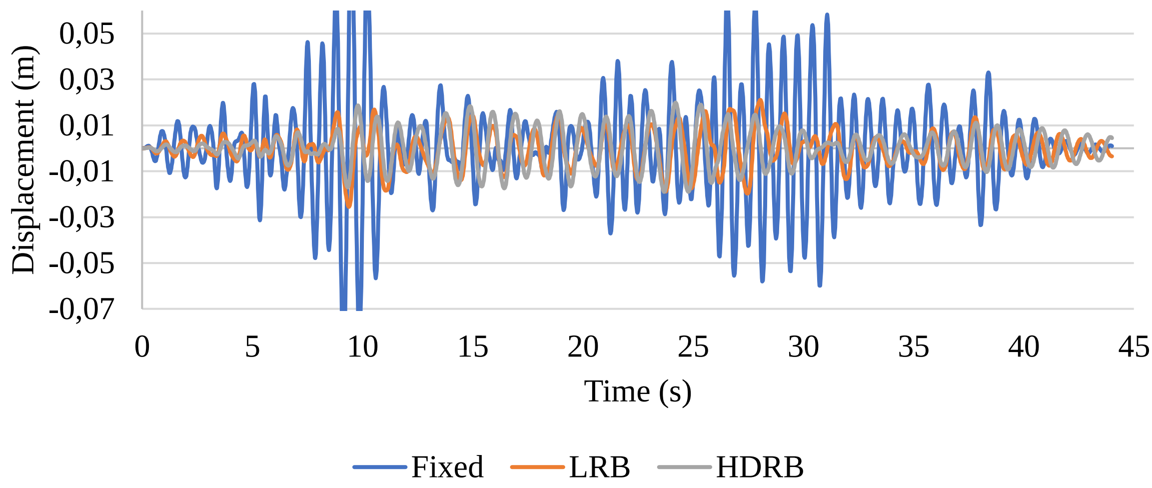

Figure 4.22 : Top-story displacement–time plots under the Landers Earthquake with reduced material strength.

In Figure 4.23, the story velocity distributions for fixed-base, LRB, and HDRB systems with reduced material strength are presented, while Figure 4.24 shows the corresponding velocity–time histories. For the Landers earthquake record, the fixed-base structure with reduced material strength exhibits increased relative story velocity demands, especially toward the upper stories, reflecting a more flexible structural response. In contrast, the LRB- and HDRB-isolated models show consistently low and well-distributed relative velocities along the building height, even when material strength is reduced. This behavior indicates that the dynamic response of the isolated systems is mainly controlled by the isolation mechanism, while the influence of superstructure properties remains secondary. Although the HDRB system yields slightly higher velocity demands compared to LRB, both isolation systems significantly outperform the fixed-base configuration.

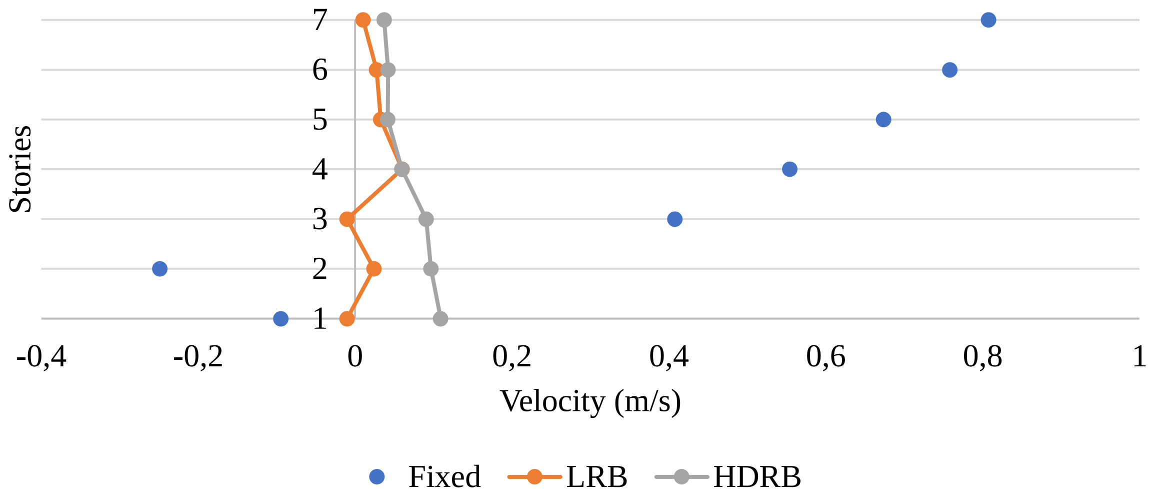

Figure 4.23 : Distribution of maximum velocities under the Landers Earthquake with reduced material strength.

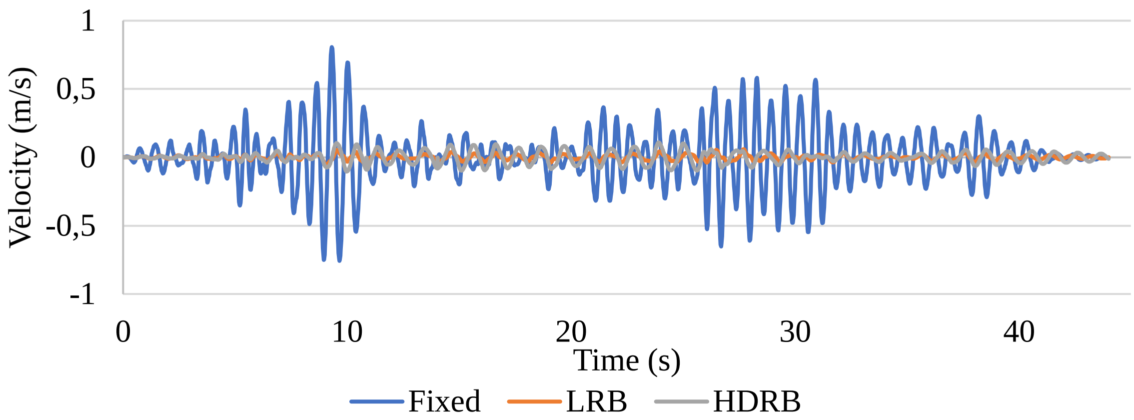

Figure 4.24 : Top-story velocity–time plots under the Landers Earthquake with reduced material strength.

Figure 4.25 presents the maximum story acceleration distributions for the fixed-base, LRB, and HDRB systems under the Landers earthquake with reduced material strength, while Figure 4.26 shows the corresponding acceleration–time histories for the top story. For the Landers earthquake record, relative story acceleration results show a pronounced amplification in the fixed-base configuration, with acceleration demands increasing rapidly toward the upper stories. This amplification becomes more evident in the model with reduced material strength, indicating a higher sensitivity of the fixed-base system to intense, long-duration ground motions such as Landers. In contrast, both LRB- and HDRB-isolated models exhibit a substantial reduction in floor acceleration levels, with limited fluctuation in the building's height. The acceleration response of the isolated structures remains largely stable even under reduced material strength conditions, highlighting that the dynamic response is primarily controlled by the isolation system rather than the superstructure properties. Among the isolation systems, HDRB provides slightly lower acceleration demands at most story levels, confirming its superior effectiveness in acceleration control under strong ground motion.

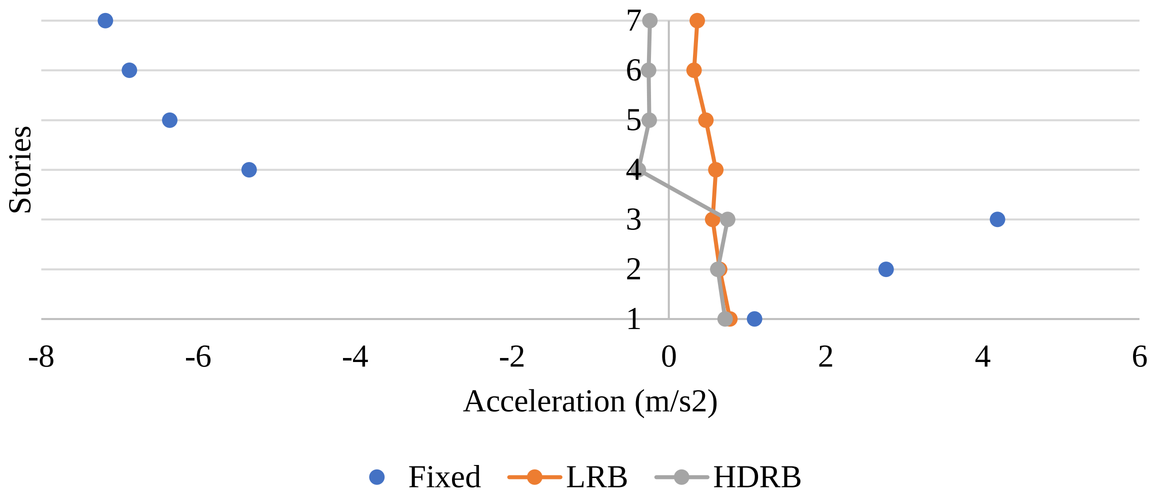

Figure 4.25 : Distribution of maximum story accelerations under the Landers Earthquake with reduced material strength.

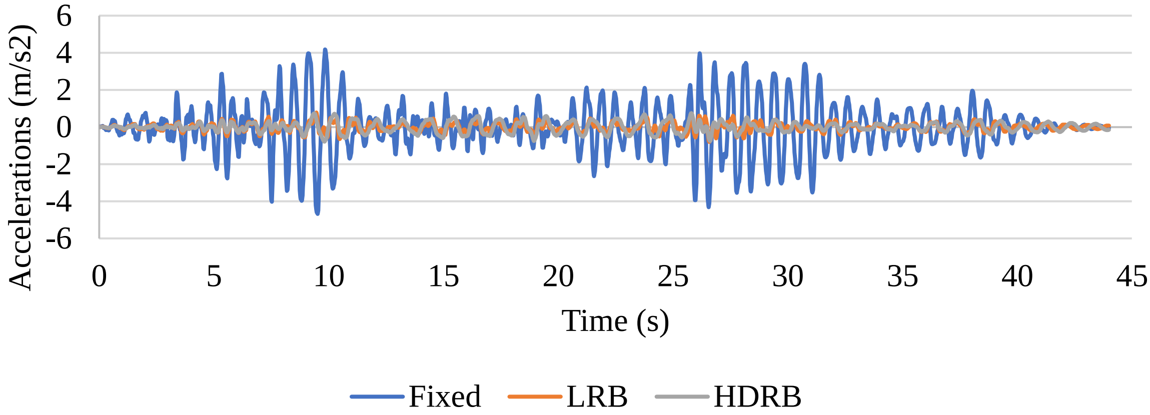

Figure 4.26 : Top-story acceleration–time plots under the Landers Earthquake with reduced material strength.

5. CONCLUDING REMARKS AND RECOMMENDATIONS

In this work, fixed-base models and models with LRB and HDRB seismic isolation systems were used to compare the seismic performance of a seven-story building. Limiting inter-story and base displacements and accelerations, as well as lowering base responses and internal forces in structural parts, are the main advantages of seismic isolation. The earthquake records used in the analyses were selected according to the seismic spectra defined by AFAD and matched using the SeismoMatch program. Additionally, seismic records sourced from the PEER database, including the Kocaeli and Landers earthquakes, were used in time-history studies, demonstrating that the structural responses of isolated and fixed-base systems differ under varying ground motion characteristics.

In addition to the reference configuration, a second set of analyses was performed using models with reduced material strength in order to represent the behavior of existing building stock. This approach enables the evaluation of seismic isolation effectiveness not only for newly designed structures but also for buildings with limited material capacity due to aging, construction deficiencies, or outdated design practices.

The structural period of the fixed-base building was determined as 0.60 s, whereas the LRB-isolated model exhibited a period of 1.77 s, corresponding to an increase of approximately 195% relative to the fixed-base structure. The HDRB-isolated model further extended the fundamental period to 2.38 s, representing an increase of about 297%. According to these results, adding seismic isolation devices considerably extends the building's fundamental period, which lowers the structure's total stiffness. The increase in the structural period alters the manner in which earthquake energy is transmitted to the structure, leading to substantial reductions in base forces and noticeable changes in story accelerations. In particular, the larger period shifts associated with the HDRB system result in more pronounced modifications to the seismic response when compared to the LRB system . Base moments, base shear forces, story accelerations, and displacements were significantly reduced in the LRB and HDRB isolated models compared to the fixed-base model. Base moments and shear forces were larger in the fixed-base model in the Kocaeli earthquake analysis, but they were lower in the LRB and HDRB models. Similarly, analyses using the Landers earthquake demonstrated that the fixed-base model produced higher accelerations and shear forces, while these values were notably reduced in the isolated models.

When reduced material strength conditions were considered, fixed-base models showed a clear increase in force and deformation demands, indicating a higher sensitivity of conventional systems to material degradation. In contrast, the seismic response of the base-isolated models was only marginally affected by the reduction in material strength, demonstrating that the overall behavior of isolated structures is predominantly governed by the isolator properties rather than the superstructure capacity.

Significant reductions in base moments and shear forces were observed in both LRB and HDRB models. In the HDRB system, this reduction was more pronounced due to its high damping capacity. The technical parameters of the isolators played a decisive role in performance, and the performance differences between the two systems were directly related to these parameters. HDRB isolators, with a balanced combination of elastomer stiffness and damping capacity, dissipate earthquake energy, while LRB isolators, consisting of a lead core combined with elastomer layers, increase energy dissipation and improve the overall response of the structure, particularly under long-period motions. In terms of deformation behavior, the fixed-base structure shows a continuous increase in relative story displacements with height, indicating a concentration of seismic effects within the superstructure. In contrast, base-isolated systems redistribute seismic demands toward the isolation level, thereby limiting deformation demands in the upper stories. This behavior was consistently observed for both the reference and reduced material strength models, confirming the robustness of seismic isolation systems under varying structural conditions.

In conclusion, this study demonstrates that seismic isolation systems increase the structural period, reduce base moments and shear forces, and lower story accelerations and velocities. A comparative evaluation of the isolation systems indicates distinct performance characteristics. While both isolation systems enhance seismic response, the HDRB system provides more effective control of structural deformations and force demands within the superstructure. This improved performance is attributed to the higher inherent damping capacity and more stable hysteretic behavior of HDRB isolators, which allow for a smoother and more uniform dissipation of seismic energy. The LRB system, although effective, exhibits relatively higher deformation demands due to its energy dissipation mechanism relying partly on yielding behavior.The HDRB system can help reduce accelerations and velocities due to its high damping capacity, while the LRB system may improve performance under long-period ground motions by increasing energy dissipation. These findings suggest that isolation systems could be considered in earthquake-prone regions to mitigate structural loads and enhance energy dissipation. Overall, the results clearly indicate that seismic isolation systems maintain their effectiveness even under reduced material strength conditions, highlighting their strong potential not only for new construction but also for the seismic upgrading of existing building stock in earthquake-prone regions. Future studies may extend this research by considering a wider range of earthquake records, different isolator types, soil–structure interaction effects, long-term performance issues such as aging and temperature variations, and economic feasibility analyses to provide a more comprehensive assessment of seismic isolation systems.

REFERENCES

Abrar, O., & Tuhta, S. (2022). Performance of elastomeric seismic isolators under long-period earthquakes. Magazine of Civil Engineering, 110(2), Article 11014. https://doi.org/10.34910/MCE.110.1

Ashokkumar, P. M., Gupta, S., & Gupta, P. K. (2025). Seismic performance of inter storey isolated and base isolated building. Asian Journal of Civil Engineering. https://doi.org/10.1007/s42107-025-01514-.

Agrawal, A., Verma, M., & Kumar, A. (2025). Comparative analysis of using rubber isolator and friction isolator in G+8 building by SAP 2000. Journal of Polymer & Composites (JoPC), 13(Special Issue 1), 479–487. https://journals.stmjournals.com/jopc/article=2024/view=190065

Al-Janabi, M. A. Q., Al-Jeznawi, D., Yang, T. Y., Bernardo, L. F. A., & Andrade, J. M. d. A. (2025). Enhancing Structural Resilience for Sustainable Infrastructure: A Global Review of Seismic Isolation and Energy Dissipation Practices. *Sustainability*, *17*(16), 7314. https://doi.org/10.3390/su17167314

Babu, S. A., & Zubedi, A. (2019). Study on soil structure interaction and base isolated system for seismic performance of structures resting on different types of soils. International Journal of Engineering Development and Research (IJEDR), 7(4). http://www.ijedr.org/ISSN2321-9939.html

Baidya, S., & Roy, B. K. (2024). Response Mitigation of Building Isolated by Shape Memory Alloy Rubber Bearing Considering Soil Structure Interaction Effect. Journal of Vibration Engineering & Technologies. https://doi.org/10.1007/s42417-024-01476-z

Baidya, S., & Roy, B. K. (2023). Comparative seismic performance of building with Cu-Al-Be and Ni-Ti SMARB seismic isolation system using particle swarm optimization. Journal of Structural Integrity and Maintenance, 1–7. https://doi.org/10.1080/24705314.2023.2170124

Castillo, B., Vides, S. M., Marulanda, J., Ortiz, A. R., & Thomson, P. (2024). Seismic performance assessment of a low-rise Thin Reinforced Concrete Wall building with Unconnected Fiber Reinforced

Elastomeric Isolators using Real-Time Hybrid Simulations. Journal of Building Engineering, 109303.

Catlioglu, O. (2021). Earthquake performance and Project budget comparison of a conventional building and a seismically isolated building. (Master's Thesis).

Cercevik, A. E., & Cercevik, N. K. (2025). Energy-Based Optimization of Seismic Isolation Parameters in RC Buildings Under Earthquake Action Using GWO. *Applied Sciences*, 15(5), 2870. https://doi.org/10.3390/app15052870

Chanda, A., & Debbarma, R. (2020). Probabilistic seismic analysis of base isolated buildings considering near and far field earthquake ground motions. Structure and Infrastructure Engineering, 1–12. https://doi.org/10.1080/15732479.2020.1836000

Chang, C.-M., Shia, S., & Yang, C.-Y. (2018). Use of active control algorithm for optimal design of base-isolated buildings against earthquakes. Structural and Multidisciplinary Optimization, 58(2), 613–626. https://doi.org/10.1007/s00158-018-1913-7

Chen, P., Lu, Y., Wang, B., Zhuang, P., & Dai, K. (2025). Enhancing seismic resilience in base-isolated structures: A performance-based comparison of HDRB and LRB isolation systems. Engineering Structures, 342, 120945. https://doi.org/10.1016/j.engstruct.2025.120945

Chen, X., Yang, H. T. Y., Shan, J., Hansma, P. K., & Shi, W. (2016). Bio-Inspired Passive Optimized Base-Isolation System for Seismic Mitigation of Building Structures. Journal of Engineering Mechanics, 142(1), 04015061. https://doi.org/10.1061/(ASCE)EM.1943-7889.0000971

Constantinou, M. C., Soong, T. T., & Dargush, G. F. (1998). *Passive energy dissipation systems for structural design and retrofit* (Monograph No. 1). Multidisciplinary Center for Earthquake Engineering Research.

Constantinou, M. C., Whittaker, A. S., Kalpakidis, Y., Fenz, D. M., & Warn, G. P. (2007). Performance of seismic isolation hardware under service and seismic loading (Technical Report No. MCEER-07). State University of New York at Buffalo.

D. Losanno, I.E. Madera Sierra, M. Spizzuoco, J. Marulanda, P. Thomson, Experimental performance of unbonded polyester and carbon fiber reinforced elastomeric isolators under bidirectional seismic excitation, Eng. Struct. 209 (November 2019) (2020) 110003, https://doi.org/10.1016/j. engstruct.2019.110003.

Deringol, A. H., & Guneyisi, E. M. (2021). Effect of Using High Damping Rubber Bearings for Seismic Isolation of the Buildings. International Journal of Steel Structures. https://doi.org/10.1007/s13296-021-00530-w

Deringol, A. H., & Guneyisi, E. M. (2023). Enhancing the seismic performance of high-rise buildings with lead rubber bearing isolators. Turkish Journal of Engineering, 7(2), 99–107. https://doi.org/10.31127/tuje.1026994

De Domenico, D., Ricciardi, G., & Zhang, R. (2020). Optimal design and seismic performance of tuned fluid inerter applied to structures with friction pendulum isolators. Soil Dynamics and Earthquake Engineering, 132, 106099. https://doi.org/10.1016/j.soildyn.2020.106099

Domadzra, Y., Bhandari, M., & Hasan, M. (2024). Seismic response of base-isolated buildings: exploring isolator properties. Asian Journal of Civil Engineering. https://doi.org/10.1007/s42107-024-01041-9

Erdik, M. (2021). Seismic isolation in Turkey. Proceedings of the Türkiye Deprem Mühendisliği Konferansı, 2-3 Haziran 2021, İstanbul, Türkiye.

Falborski, T., & Jankowski, R. (2017). Experimental Study on Effectiveness of a Prototype Seismic Isolation System Made of Polymeric Bearings. Applied Sciences, 7(8), 808. https://doi.org/10.3390/app7080808

Ganji, M., & Kazem, H. (2017). Comparing Seismic Performance of Steel Structures Equipped with Viscous Dampers and Lead Rubber Bearing Seismic isolation under Near-Field Earthquake. Civil Engineering Journal, 3(2), 124–136. https://doi.org/10.28991/cej-2017-00000079

Gao, H., Wang, H., Li, J., Wang, Z., Liang, R., Xu, Z., & Ni, Y. (2021). Optimum design of viscous inerter damper targeting multi-mode vibration mitigation of stay cables. *Engineering Structures*, *226*, 111375. https://doi.org/10.1016/j.engstruct.2020.111375

Gowda Kiran, K. K., & Noroozinejad Farsangi, E. (2020). Performance Evaluation of the Seismic isolation Technique on the Blast Mitigation of Spatial Structures. Civil and Environmental Engineering Reports, 30(3), 134–160. https://doi.org/10.2478/ceer-2020-0037

Gutierrez Soto, M., & Adeli, H. (2018). Vibration control of smart base-isolated irregular buildings using neural dynamic optimization model and replicator dynamics. *Engineering Structures*, *156*, 322–336. https://doi.org/10.1016/j.engstruct.2017.09.037

Habib, A., AL Houri, A., & Yildirim, U. (2021). Comparative study of base-isolated irregular RC structures subjected to pulse-like ground motions with low and high PGA/PGV ratios. Structures, 31, 1053–1071. https://doi.org/10.1016/j.istruc.2021.02.021

He, W., Zhou, Y., Wang, Z., Xu, H., & Ning, X. (2024). Soil-dependent stochastic optimization of seismic isolation system with negative stiffness inerter damper subjected to non-stationary seismic excitation. Structures, 67, 106955. https://doi.org/10.1016/j.istruc.2024.106955

He, W., Qiao, J., Ye, K., & Xu, H. (2023). Design optimization of hybrid isolation bearing for base-isolated buildings catering to multi-level performance fortification criteria. *Structures*, *58*, 105511. https://doi.org/10.1016/j.istruc.2023.105511

Hu, J. (2014). Response of Seismically Isolated Steel Frame Buildings with Sustainable Lead-Rubber Bearing (LRB) Isolator Devices Subjected to Near-Fault (NF) Ground Motions. Sustainability, 7(1), 111–137. https://doi.org/10.3390/su7010111

Ibrahim, O. (2025). Resilience of hospital structures under seismic loads: A case study informed by the 2023 Maraş earthquake. Structures, 74, 108642. https://doi.org/10.1016/j.istruc.2025.108642

Islam, A. B. M. S., & Al-Kutti, W. A. (2018). Seismic response variation of multistory base-isolated buildings applying lead rubber bearings. Computers and Concrete, 21(5), 495–504. https://doi.org/10.12989/cac.2018.21.5.495

Islam, A. B. M. S., Jameel, M., Jumaat, M.Z. (2011). Seismic isolation in buildings to be a practical reality: behavior of structure and installation technique. Journal of Engineering and Technology Research, 3(4), 99-117.

Istanbul Metropolitan Municipality (IMM), Department of Earthquake and Ground Research. (2011, December). Geology of the Istanbul Provincial Area.

Jasim, F. A., Jasim, N. A., & Al-Hussein, A. A. (2024). Advancing seismic performance: Isolators, TMDs, and multi-level strategies in reinforced concrete buildings. Open Engineering, 14(1). https://doi.org/10.1515/eng-2022-0589

Kaatsız, K., Alıcı, F. S., Sucuoglu, H., Tanıser, S., & Kale, Ö. (2024). Seismic performance assessment of seismic isolation systems in five hospitals during the Mw7.8 and Mw7.6 2023 earthquakes in Southeast Turkey. Earthquake Spectra. https://doi.org/10.1177/87552930241284613

Kandemir, E. C., & Mortazavi, E. (2024). Optimizing seismic isolation system parameters using a fuzzy reinforced butterfly optimization: A case study of the 2023 Kahramanmaras earthquake sequence. Journal of Vibration and Control, 30(3-4), 502-512. https://doi.org/10.1177/10775463231217356

Kim, I.-H., Jung, H.-J., & Koo, J.-H. (2010). Experimental evaluation of a self-powered smart damping system in reducing vibrations of a full-scale stay cable. Smart Materials and Structures, 19(11), 115027. https://doi.org/10.1088/0964-1726/19/11/115027

Kumar, H., & Saha, S. K. (2021). Seismic Performance of Base-Isolated Elevated Liquid Storage Tanks Considering Soil–Structure Interaction. Practice Periodical on Structural Design and Construction, 26(1), 04020062. https://doi.org/10.1061/(asce)sc.1943-5576.0000545

Lai, Z., Luo, B., Shuang, C., Cao, W., Tan, P., Shu, W., & Zhu, Z. (2025). Seismic performance of isolation structure with double-sided sliding horizontal-vertical decoupling bearing. Structures, 79, 109579. https://doi.org/10.1016/j.istruc.2025.109579

Liu, Y., Li, J., & Lin, G. (2024). Seismic mitigation analysis of three-dimensional base-isolated nuclear structures with soil-dependent isolation system under extreme earthquakes. Engineering Structures, 311, 118187. https://doi.org/10.1016/j.engstruct.2024.118187

Lo Frano, R. (2018). Benefits of Seismic Isolation for Nuclear Structures Subjected to Severe Earthquake. Science and Technology of Nuclear Installations, 2018, 1–11.

Madhukumar, M., Santhi M, H., & V, V. (2022). Performance analysis of lead rubber bearing isolation system for low, medium and high- rise RC buildings. Research on Engineering Structures and Materials. https://doi.org/10.17515/resm2022.437ie0526

Manchalwar, A., & Bakre, S. V. (2020). Seismic Performance of Structure with Isolated Foundation Using U-Shape Steel Damper as an Isolator. Soil Mechanics and Foundation Engineering, 57(2), 170–177.

Manna, R., Elias, S., & Matsagar, V. (2024). Response of Base-Isolated Building with Secondary System under Earthquakes and Pulse-Type Ground Motions. Practice Periodical on Structural Design and Construction, 29(4). https://doi.org/10.1061/ppscfx.sceng-1504

Md, Z. N., S.C., M., & Jyosyula, S. K. R. (2024). Performance of low-cost unreinforced elastomeric isolator for masonry building: Experimental investigations and numerical analysis. Structures, 63, 106365. https://doi.org/10.1016/j.istruc.2024.106365

Mohebbi, M., & Dadkhah, H. (2017). Multi-Objective Semi-Active Seismic isolation System. International Journal of Optimization In Civil Engineering, 7(3), 319-338.

Mohebbi, M., & Dadkhah, H. (2019). Optimal Smart Seismic isolation System for Multiple Earthquakes. International Journal of Optimization In Civil Engineering, 9(1), 19-37.

Mortazavi, A., & Kandemir, E. Ç. (2024). Simultaneous optimization of capacity and topology of seismic isolation systems in multi-story buildings using a fuzzy reinforced differential evolution method. Advances in Engineering Software, 198, 103781. https://doi.org/10.1016/j.advengsoft.2024.103781

Narhare, M., & Kasnale, A. (2019). A review of behaviour of building under earthquake with or without seismic isolation. International Research Journal of Engineering and Technology (IRJET), 6(7).

Nasery, M. M., Ergun, M., Ates, S., & Husem, M. (2015). Comparing the dynamic behavior of a hospital-type structure with fixed and isolated base. Earthquakes and Structures, 9(3), 657–671. https://doi.org/10.12989/eas.2015.9.3.657

Ozer, E., & Inel, M. (2021). The effect of seismic isolation on performance of a residence building. Pamukkale University Journal of Engineering Sciences, 27(3), 304–312. https://doi.org/10.5505/pajes.2020.36825

Ozer, E., & Inel, M. (2025). The effect of single and combined use of base isolator and fluid viscous damper on seismic performance in a conventional RC building with torsional irregularity. Journal of Building Engineering, 101, 111898. https://doi.org/10.1016/j.jobe.2025.111898

Ozer, E., Inel, M., & Cayci, B. T. (2022). Seismic Performance Comparison of Fixed and Base-Isolated Models. Iranian Journal of Science and Technology, Transactions of Civil Engineering. https://doi.org/10.1007/s40996-022-00936-4

Republic of Turkey Ministry of Environment and Urbanization. (2018). Türkiye Bina Deprem Yönetmeliği [Turkish Building Earthquake Code (TSC 2018)]. Resmî Gazete, No. 30364, March 18, 2018. (in Turkish)

Sadek, F., Mohraz, B., Taylor, A. W., & Chung, R. M. (1996). *Passive energy dissipation devices for seismic applications* (NIST Technical Note No. 1458). U.S. Department of Commerce, National Institute of Standards and Technology.

Salaas, B., Bekdaş, G., Ibrahim, Y. E., Nigdeli, S. M., Ezzat, M., Nawar, M., & Kayabekir, A. E. (2023). Design Optimization of a Hybrid Vibration Control System for Buildings. *Buildings*, 13(4), 934. https://doi.org/10.3390/buildings13040934

Sapountzakis, E., Florakis, G., & Kapasakalis, K. (2024). Design and Performance Assessment of Base Isolated Structures Supplemented with Vibration Control Systems. *Buildings*, *14*(4), 955. https://doi.org/10.3390/buildings14040955

Saritas, F., Bedirhanoglu, I., Konak, A., & Keskin, M. S. (2022). Effect of Seismic Isolation on the Performance of High-Rise Buildings with Torsional Instability. Sustainability, 15(1), 36. https://doi.org/10.3390/su15010036

Scruggs, J. T., Taflanidis, A. A., & Beck, J. L. (2006). Reliability-based control optimization for active seismic isolation systems. Structural Control and Health Monitoring, 13(2-3), 705–723. https://doi.org/10.1002/stc.107

Sengel, H. S., Erol, H., & Yavuz, E. (2009). Seismic isolation technique and sample experiment related to its use. Journal of Engineering and Architecture Faculty of Eskişehir Osmangazi University, 22(2).

Shang, J., Tan, P., Zhang, Y., Han, J., & Mi, P. (2021). Seismic isolation design of structure using variable friction pendulum bearings. Soil Dynamics and Earthquake Engineering, 148, 106855. https://doi.org/10.1016/j.soildyn.2021.106855

Sheng, Y., Yang, Z., Meng, Y., & Jia, B. (2024). A Study on the Design of a New Three-Dimensional Seismic Isolation Bearing Based on an Improved Genetic Algorithm for Bridge Engineering. Applied Sciences, 14(20), 9453. https://doi.org/10.3390/app14209453

Siringoringo, D. M., & Fujino, Y. (2014). Seismic response analyses of an asymmetric base-isolated building during the 2011 Great East Japan (Tohoku) Earthquake. Structural Control and Health Monitoring, 22(1), 71–90. https://doi.org/10.1002/stc.1661

Sugihardjo, H., & Lesmana, Y. (2019). The seismic performance of residential housing under strong earthquake shaking. International Journal of Civil Engineering and Technology, 10(1), 2195–2209. https://www.iaeme.com/ijciet/issues.asp?JType=IJCIET&VType=10&IType=1

Sulthan, F., & Seki, M. (2023). Seismic fragility analysis of seismic isolation reinforced concrete structure building considering performance – a case study for Indonesia. Structural Monitoring and Maintenance, 10(3), 243–260. https://doi.org/10.12989/smm.2023.10.3.243

Thakur, R., & Tiwary, A. K. (2023). Comparative study on the effectiveness of fluid viscous dampers and seismic isolation: an approach toward enhancing seismic performance of composite structures. Innovative Infrastructure Solutions, 8(10). https://doi.org/10.1007/s41062-023-01229-z

TS 498, (1987). Design Loads for Buildings. Turkish Standards Institute (TSE), Ankara, Türkiye.

TS 500, (2000). Requirements for Design and Construction of Reinforced Concrete Structures. Turkish Standards Institute (TSE), Ankara, Türkiye.

TS 708, (2010). Steel for the Reinforcement of Concrete - Reinforcing Steel. Turkish Standards Institute (TSE), Ankara, Türkiye.

Usta, P. (2021). Investigation of a Base-Isolator System's Effects on the Seismic Behavior of a Historical Structure. Buildings, 11(5), 217. https://doi.org/10.3390/buildings11050217

Ye, K., & Nyangi, P. (2021). Enhancing the seismic performance of dual-isolated structure with optimal supplemental inerters. Bulletin of Earthquake Engineering.

Yuan, W., Xie, B., Zhou, W., Yin, Z., Wang, Z., & Ding, T. (2025). Seismic performance analysis of wind and rain bridge structures and design of a seismic vibration damping program using rubber isolators. Structures, 79, 109474. https://doi.org/10.1016/j.istruc.2025.109474

Zhong, W., Li, B., Liu, Y., Tan, P., & Zhou, F. (2024). The effect of an improved passive bumper on the seismic response of the base-isolated structure: Numerical simulations and optimization design. *Soil Dynamics and Earthquake Engineering*, 176, 108335. https://doi.org/10.1016/j.soildyn.2023.108335

Ziraoui, A., Kissi, B., Aaya, H., & Azdine, I. (2024). Seismic behavior of base-isolated building structures with lead rubber bearings (LRBs). Procedia Structural Integrity, 61, 171–179. https://doi.org/10.1016/j.prostr.2024.06.023

Whittaker, A. S., Sollogoub, P., & Kim, M. K. (2018). Seismic isolation of nuclear power plants: Past, present and future. Nuclear Engineering and Design, 338, 290–299. https://doi.org/10.1016/j.nucengdes.2018.07.025

Url-1 < https://www.usgs.gov/programs/earthquake-hazards/cool-earthquake-facts>, retrieved 21.11.2025.

Url-2 < https://www.bridgestone.com/products/diversified/antiseismic_rubber.html>, retrieved 21.11.2025.

Url-3 < https://www.emke.com.tr/urunlerimiz/kaucuk-izolator-nrb>, retrieved 21.11.2025.

Url-4 < https://www.mageba-group.com/tr/tr/1026/Binalar/Seizmicki-uredaji/LASTO-HDRB/LASTO-HDRB.htm>, retrieved 21.11.2025.

Url-5 < https://arfenbrb.com/sismik-izolatorler>, retrieved 21.11.2025.

Url-6<https://www.enr.com/articles/42366-the-10-largest-base-isolated-buildings-in-the-world>, retrieved 21.11.2025.

Url-7 < https://www.afad.gov.tr >, retrieved 21.11.2025.

Url-8 <https://fagosismikizolasyon.com/lrb-lead-rubber-bearing/>, retrieved 21.11.2025.

APPENDICES

APPENDIX A: DVD containing results and computer program

CURRICULUM VITAE

Demet OKUROĞLU

EDUCATION

- **B.Sc. :** 2020, Istanbul Technical University, Civil Engineering, Structural Engineering

PUBLICATIONS, PRESENTATIONS AND PATENTS ON THE THESIS:

- **Okuroglu D., Yanik A.** 2025: The Effect of Seismic Isolation Systems on Structural Behavior: A Literature Review. ICHEAS 10th International Conference On Health, Engineering And Applied Sciences November 1 - 3, 2025 Dubai